J|A|C|S ARTICLES

Published on Web 04/01/2010

"Chain-Like" Trimetallic Ruthenium Complexes with C_7 Carbon-Rich Bridges: Experimental and Theoretical Investigations of Electronic Communication Tuning in Five Distinct Oxidation States

Céline Olivier,[†] Karine Costuas,*[,†] Sylvie Choua,*[,‡] Vincent Maurel,[‡] Philippe Turek,[‡] Jean-Yves Saillard,[†] Daniel Touchard,[†] and Stéphane Rigaut*[,†]

UMR 6226 CNRS−Université de Rennes 1, Sciences Chimiques de Rennes, Campus de Beaulieu, F-35042 Rennes Cedex, France, and UMR 7177 CNRS−Université de Strasbourg, Institut de Chimie, 1 rue Blaise Pascal, BP 296 R8, F-67008 Strasbourg Cedex, France

Received October 27, 2009; E-mail: stephane.rigaut@univ-rennes1.fr; karine.costuas@univ-rennes1.fr; sylvie.choua@unistra.fr

Abstract: In this work, we report the synthesis and the electronic properties of the unique highly conjugated molecular wires *trans*-[Cl−(dppe)$_2$Ru═C═C═(Ph)C−CH═(CH$_3$)C−C≡C−(X)$_2$Ru−C≡C−C(CH$_3$)═CH−C(Ph)═C═C═Ru(dppe)$_2$Cl]$^{n+}$ (n = 2, X = dppe ([**3a**](OTf)$_2$) and dppm ([**3b**](OTf)$_2$) with three similar metal centers spanned by two odd-numbered unsaturated C_7 chains providing a 28 Å long conjugated path and displaying five well-separated redox states (n = 0−4). Successive one-electron transfer steps were studied by means of cyclic voltammetry, EPR and UV−vis−NIR−IR spectroelectrochemistry. The electronic and physical properties of the different states were further rationalized with the help of DFT-based calculations. Upon one-electron reduction (n = 1), the single electron is delocalized over the two carbon chains through the central metal atom to an extent driven by the rotations within and between the chains. The second reduction (n = 0) involves the whole carbon-rich conjugated path of the molecule in a spin polarized scheme: one electron is delocalized over each chain, and the two electrons are antiferromagnetically coupled with a coupling on the order of kT. Interestingly, oxidation processes strongly involve both the metal atoms and the bridging ligands. The combined investigations reveal that the mono-oxidized system (n = 3) presents a spin density uniformly distributed between the metal atoms and the carbon atoms of the chains, whereas in the second oxidation state (n = 4) the compounds show a strong antiferromagnetic coupling on the order of 4 kT between the two single electrons localized in two distinct delocalized spin orbitals implying all the carbon atoms of the bridges and the three metal atoms. Thus, for the first time, electronic communication was fully evidenced and tuned in homonuclear trimetallic oligomeric carbon-rich systems in either an oxidation or a reduction process.

Introduction

Identification and control of the influencing factors for electron transfer over nanometric distances will be a decisive achievement for the fundamental understanding of the processes and therefore for the design of molecular-scale electronic devices such as molecular wires.[1,2] For this purpose, redox-active metal complexes including a bridging ligand between the redox centers are particularly suitable as they afford stable delocalized mixed-valence (MV) states at low potential, under carefully controlled conditions, and electronic communication can be easily assessed from common spectroscopic studies.[3,4]

Noteworthy, the huge flexibility of metal complexes can lead to a wide range of arrangements in order to induce peculiar chemical and physical properties in the system. So far, dinuclear complexes are among the most thoroughly investigated.[3−10] Electronic cooperation was also established in some complexes

[†] UMR 6226 CNRS−Université de Rennes 1.
[‡] UMR 7177 CNRS−Université de Strasbourg.

(1) (a) Joachim, C.; Ratner, M. A. *Proc. Natl. Acad. Sci., U.S.A.* **2005**, *102*, 8801–8808. (b) Nitzan, A.; Ratner, M. A. *Science* **2003**, *300*, 1384–1389. (c) Carroll, R. L.; Gorman, C. B. *Angew. Chem., Int. Ed.* **2002**, *41*, 4378. (d) *Molecular Electronics: Science and Technology*; Aviram, A., Ratner, M. A., Eds.; New York Academy of Sciences: New York, 1998; Vol. 852. (e) James, D. K.; Tour, J. M. *Top. Curr. Chem.* **2005**, *257*, 33–62.

(2) (a) McCreery, R. L. *Chem. Mater.* **2004**, *16*, 4477–4496. (b) Salomon, A.; Cahen, D.; Lindsay, S.; Tomforh, J.; Engelkes, V. B.; Frisbie, C. D. *Adv. Mater.* **2003**, *15*, 1881. (c) James, D. K.; Tour, J. *Chem. Mater.* **2004**, *15*, 4423–4435. (d) Metzger, R. M. *Chem. Rev.* **2003**, *103*, 3803–3834. (e) Lindsay, S. M.; Ratner, M. A. *Adv. Mater.* **2007**, *19*, 23–31.

(3) For reviews on electron transfer in mixed-valence systems, see: (a) Creutz, C. *Prog. Inorg. Chem.* **1983**, *30*, 1–73. (b) Brunschwig, B. S.; Creutz, C.; Sutin, N. *Chem Soc. Rev.* **2002**, *31*, 168–184. (c) Nelsen, S. F. In *Electron Transfer in Chemistry*; Balzani, V, Ed.; Wiley-VCH: Weinheim, Germany, 2001; Vol. 1, Chapter 10. (d) Launay, J.-P.; Coudret, C. In *Electron Transfer in Chemistry*; Balzani, V., Ed.; Wiley-VCH: Weinheim, Germany, 2001; Vol. 5, Chapter 1. (e) Launay, J.-P. *Chem. Soc. Rev.* **2001**, *30*, 386–397. (f) Demadis, K. D.; Hartshorn, C. M.; Meyer, T. J. *Chem. Rev.* **2001**, *101*, 2655–2685. (g) Ceccon, A.; Santi, S.; Orian, L.; Bisello, A. *Coord. Chem. Rev.* **2004**, *248*, 683–724. (h) D'Alessandro, D. M.; Keene, F. R. *Dalton Trans.* **2006**, 424–440.

(4) Astruc, D. *Electron Transfer and Radical Processes in Transition Metal Chemistry*; VCH: New York, 1995.

10.1021/ja908948g

with more than two redox centers[11] such as star-shaped,[12] square, or triangle[13,14] metallamacrocyclic complexes. The elucidation of the fundamental processes in linear trinuclear complexes should provide the link between binuclear systems and metallo supramolecular oligomeric systems to devices, as linear molecules represent the majority of active materials used in molecular electronics and ultimately could find applications in molecular devices.[2,10c] If significant remote metal−metal interactions in trimetallic complexes involving pyrazine[15] or phenantrolynopyrazine ligands[16] have been addressed, as well as in assemblies involving the short cyanide bridge[17] or ferrocene,[18] nonaromatic longer bridges giving rise to strong electronic coupling are needed to engender electronic delocalization over long length scale.

Transition metal complexes containing σ-polyynyl ligands of various lengths constitute a particularly attractive class of candidates for molecular wires as they favor very efficient electronic delocalization between two metallic centers in MV complexes by matching the energy of the metal-based orbitals with appropriate bridging ligand orbitals.[6−10] The synthesis of linear conjugated monodisperse complexes with more than two metal sites should thus lead to long and efficient wires in which the metal can operate as a connector. Placing equivalent redox sites as end-cap such as ferrocene has been used to evaluate whether intramolecular electronic communication occurs through a metal-containing fragment.[19,20] We and others have demonstrated the exceptional ability of the ruthenium atom to operate as a connector allowing electron flow to occur between different elements in carbon-rich systems, providing validation of the proposal to realize oligomeric molecular wires of precisely controlled lengths using ruthenium.[20,21] Surprisingly, experimental studies on fully organometallic carbon-rich systems with more than two identical redox-active metal fragments remain particularly scarce, probably for synthetic reasons, and limited.[10d,22] The degree to which the process is influenced by nuclearity and geometry in such systems is not clear owing to the presence of

(5) (a) Chisholm, M. H.; Patmore, N. J. *Acc. Chem. Res.* **2007**, *40*, 19–27. (b) Lear, B. J.; Glover, S. D.; Salsman, J. C.; Londergan, C. H.; Kubiak, C. P. *J. Am. Chem. Soc.* **2007**, *129*, 12772–12779. (c) Cotton, F. A.; Liu, C. Y.; Murillo, C. A.; Villagrán, D.; Wang, X. *J. Am. Chem. Soc.* **2004**, *126*, 14822–14831. (d) Cotton, F. A.; Zhong, J.-Y. J.; Murillo, C. A.; Reibenspies, J. H. *Chem. Commun.* **2008**, 211–213. (e) Meacham, A. P.; Druce, K. L.; Bell, Z. R.; Ward, M. D.; Keister, J. B.; Lever, A. B. P. *Inorg. Chem.* **2003**, *42*, 7887–7896. (f) Fraysse, S.; Coudret, S.; Launay, J.-P. *J. Am. Chem. Soc.* **2003**, *125*, 5880–5888. (g) Kaim, W.; Lahiri, G. K. *Angew. Chem., Int. Ed.* **2007**, *46*, 1778–1796. (h) Kaim, W.; Sarkar, B. *Coord. Chem. Rev.* **2007**, *251*, 584–594. (i) Balzani, V.; Juris, A.; Venturi, M.; Campagna, S.; Serroni, S. *Chem. Rev.* **1996**, *96*, 759–833. (j) Ziessel, R.; Hissler, M.; El-Ghaoury, A.; Harriman, A. *Chem. Soc. Rev.* **1998**, *178−180*, 1251–1298.

(6) For reviews on organometallic complexes, see: (a) Ren, T. *Organometallics* **2005**, *24*, 4854–4870. (b) Venkatesan, K.; Blacque, O.; Berke, H. *Dalton Trans* **2007**, 1091–1100. (c) Low, P. J.; Roberts, R. L.; Cordiner, R. L.; Hartl, F. *J. Solid State Electrochem* **2005**, *9*, 717–731. (d) Paul, F.; Lapinte, C. *Coord. Chem. Rev.* **1998**, *178−180*, 431–509. (e) Bruce, M. I.; Low, P. J. *Adv. Organomet. Chem.* **2004**, *50*, 179–444. (f) Paul, F.; Lapinte, C. In *Unusual Structures and Physical Properties in Organometallic Chemistry*; Gielen, M., Willem, R., Wrackmeyer, B., Eds.; Wiley: New York, 2002; pp 220−291. (g) Szafert, S.; Gladysz, J. A. *Chem. Rev.* **2003**, *103*, 4175–4206. (h) Akita, M.; Koike, T. *Dalton Trans.* **2008**, 3523–3530. (i) Powell, C. E.; Humphrey, M. G. *Coord. Chem. Rev.* **2004**, *248*, 725–756.

(7) For representative examples with acetylide complexes, see: (a) Hamon, P.; Justaud, F.; Cador, O.; Hapiot, P.; Rigaut, S.; Toupet, L.; Ouahab, L.; Stueger, H.; Hamon, J.-R.; Lapinte, C *J. Am. Chem. Soc.* **2008**, *130*, 17372–17383. (b) Ghazala, S. I.; Paul, F.; Toupet, L.; Roisnel, T.; Hapiot, P.; Lapinte, C. *J. Am. Chem. Soc.* **2006**, *128*, 2463–2476. (c) Fox, M. A.; Roberts, R. A.; Baines, T. E.; Le Guennic, B.; Halet, J.-F.; Hartl, F.; Yufit, D. S.; Albesa-Jové, D.; Howard, J. A. K.; Low, P. J. *J. Am. Chem. Soc.* **2008**, *130*, 3566–3578. (d) Dembinski, R.; Bartik, T.; Bartik, B.; Jaeger, M.; Gladysz, J. A. *J. Am. Chem. Soc.* **2000**, *122*, 810–822. (e) Mohr, W.; Stahl, J.; Hampel, F.; Gladysz, J. A. *Chem.−Eur. J.* **2003**, *9*, 3324–3340. (f) Kheradmandan, S.; Venkatesan, K.; Blacque, O.; Schmalle, H. W.; Berke, H. *Chem.−Eur. J.* **2004**, *10*, 4872–4885. (g) Xu, G.-L.; Zou, G.; Ni, Y.-H.; De Rosa, M. C.; Crutchley, R. J.; Ren, T. *J. Am. Chem. Soc.* **2003**, *125*, 10057–10065. (h) Bruce, M. I; Low, P. J.; Costuas, K.; Halet, J.-F.; Best, S. P.; Heath, G. A. *J. Am. Chem. Soc.* **2000**, *122*, 1949–1962. (i) Zheng, Q.; Gladysz, J. A. *J. Am. Chem. Soc.* **2005**, *127*, 10508–10509. (j) Seetharaman, S. K.; Rose, D. J.; Zubieta, J.; Sponsler, M. B. *Organometallics* **2003**, *22*, 3485–3494. (k) Wong, K. T.; Lehn, J.-M.; Peng, S.-M.; Lee, G.-H. *Chem. Commun.* **2000**, 2259–2960. (l) Liu, S. H.; Hu, Q. Y.; Xue, P.; Wen, T. B.; Williams, I. D.; Jia, G. *Organometallics* **2005**, *24*, 769–772. (m) Pichlmaier, M.; Winter, R. F.; Zabel, M.; Zalis, S. *J. Am. Chem. Soc.* **2009**, *131*, 4895–4903. (n) Akita, M.; Tanaka, Y.; Naitoh, C.; Ozawa, T.; N; Hayashi, N.; Takeshita, M.; Inagaki, A.; Chung, M.-C. *Organometallics* **2006**, *25*, 5261–5275. (o) Mantovani, N.; Brugnati, M.; Gonsalvi, L.; Grigiotti, E.; Laschi, F.; Marvelli, L.; Peruzzini, M.; Reginato, G.; Rossi, R.; Zanello, P *Organometallics* **2005**, *24*, 405–418. (p) Sakurai, A.; Akita, M.; Moro-Oka, Y. *Organometallics* **1999**, *18*, 3241–3244. (q) Gil-Rubio, J.; Werberndörfer, B.; Werner, H. *Angew. Chem., Int. Ed.* **2000**, *39*, 786–789.

(8) Rigaut, S.; Touchard, D.; Dixneuf, P. H. *Coord. Chem. Rev.* **2004**, 1586–16501.

(9) (a) Rigaut, S.; Le Pichon, L.; Daran, J.-C.; Touchard, D.; Dixneuf, P. H. *Chem. Commun.* **2001**, 1206–1207. (b) Rigaut, S.; Massue, J.; Touchard, D.; Fillaut, J.-L.; Golhen, S.; Dixneuf, P. H. *Angew. Chem., Int. Ed.* **2002**, *41*, 4513–4517. (c) Rigaut, S.; Olivier, C.; Costuas, K.; Choua, S.; Fadhel, O.; Massue, J.; Turek, P.; Saillard, J. Y.; Dixneuf, P. H.; Touchard, D. *J. Am. Chem. Soc.* **2006**, *128*, 5859–5878. (d) Vacher, A.; Benameur, A.; Mback Ndiaye, C.; Touchard, D.; Rigaut, S. *Organometallics* **2009**, *28*, 6096–6100.

(10) (a) Gauthier, N.; Olivier, C.; Rigaut, S.; Touchard, D.; Roisnel, T.; Humphrey, M. G.; Paul, F. *Organometallics* **2008**, *26*, 1063–1072. (b) Liu, Y.; Lagrost, C.; Costuas, K.; Tchouar, N.; Le Bozec, H. ; Rigaut, S. *Chem. Commun.* **2008**, 6117–6119. (c) Kim, B.; Beebe, J. M.; Olivier, C.; Rigaut, S.; Touchard, D.; Kushmerick, J. G.; Zhu, X.-Y.; Frisbie, C. D. *J. Phys. Chem. C* **2007**, *111*, 7521–7526. (d) Olivier, C.; Kim, B.-S.; Touchard, D.; Rigaut, S. *Organometallics* **2008**, *27*, 509–518. (e) Rigaut, S.; Perruchon, J.; Le Pichon, L.; Touchard, D.; Dixneuf, P. H. *J. Organomet. Chem.* **2003**, *670*, 37–44. (f) Rigaut, S.; Touchard, D.; Dixneuf, P. H. *Organometallics* **2003**, *22*, 3980–3984. (g) Rigaut, S.; Perruchon, J.; Guesmi, S.; Fave, C.; Touchard, D.; Dixneuf, P. H. *Eur. J. Inorg. Chem.* **2005**, 447–460.

(11) D'Alessandro, D. M.; Keene, F. R. *Chem. Rev.* **2006**, *106*, 2270–2298.

(12) For examples, see: (a) Xia, H.; Wen, T. B.; Hu, Q. Y.; Wang, X.; Chen, X.; Shek, L. Y.; Williams, I. D.; Wong, K. S.; Wong, G. K. L.; Jia, G. *Organometallics* **2005**, *24*, 562–569. (b) Long, N. J.; Martin, A. J.; White, A. J. P.; Williams, D. J.; Fontani, M.; Lashi, F.; Zanello, P. *Dalton Trans.* **2000**, *338*, 7–3392. (c) Weyland, T.; Costuas, K.; Toupet, L.; Halet, J. F.; Lapinte, C. *Organometallics* **2000**, *19*, 4228–4239. (d) Uno, M.; Dixneuf, P. *Angew. Chem., Int. Ed.* **1998**, *37*, 1714–1717. (e) Linseis, M.; Winter, R. F.; Sarkar, B.; Kaim, W.; Zalis, S. *Organometallics* **2008**, *27*, 3321–3324. (f) Packheiser, R.; Ecorchard, P.; Rüffer, T.; Lohan, M.; Bräuer, B.; Justaud, F.; Lapinte, C.; Lang, H. *Organometallics* **2008**, *27*, 3444–3457. (g) Onitsuka, K.; Ohara, N.; Takei, F.; Takahashi, S. *Dalton Trans.* **2006**, 3693–3698. (h) Yao, H.; Sabat, M.; Grimes, R. N.; Zanello, P.; Fabrizi de Biani, F. *Organometallics* **2003**, *22*, 2581–2593. (i) Jiao, J.; Long, G. J.; Rebbouh, L.; Granjean, F.; Beatty, A. M.; Fehlner, T. P. *J. Am. Chem. Soc.* **2005**, *127*, 17819–17831. (j) Althoff, A.; Eisner, D.; Jutzi, P.; Lenze, N.; Neumann, B.; Schoeller, W. W.; Stammler, H.-G. *Chem.−Eur. J.* **2006**, *12*, 5471–5480. (k) Kotz, J.; Neyhart, G.; Wining, W. J.; Rausch, M. D. *Organometallics* **1983**, *2*, 79–82. (l) D'Alessandro, D. M.; Keene, F. R. *Chem.−Eur. J.* **2005**, *11*, 3670–3688.

(13) (a) Lau, V. C.; Berben, L. A.; Long, J. R. *J. Am. Chem. Soc.* **2002**, *124*, 9042–9043. (b) Oshio, H.; Onodera, H.; Tamada, O.; Mizutani, H.; Hikichi, T.; Ito, T. *Chem.−Eur. J.* **2000**, *6*, 2523–23530. (c) Oshio, H.; Ondonera, H.; Ito, T *Chem.−Eur. J.* **2003**, *9*, 3946–3950. (d) Berben, L. A.; Faia, M. C.; Crawford, N. R.; Long, J. R. *Inorg. Chem.* **2006**, *45*, 6378–6386. (e) Nihei, M.; Ui, M.; Hoshino, N.; Oshio, H. *Inorg. Chem.* **2008**, *48*, 6106–6108. (f) Santi, S.; Orian, L.; Donoli, A.; Bisello, A.; Scapinelllo, M.; Benetollo, F.; Ganis, P.; Ceccon, A. *Angew. Chem., Int. Ed.* **2008**, *47*, 5331–5334.

multiple electronically coupled metals and to the involvement of the bridging ligands in the redox processes, which complicates the analysis.

In the light of these observations and on the basis of our earlier studies using the fragment $[RuCl(dppe)_2]^+$ (dppe = 1,2-bis(diphenylphosphino)ethane), which provides stable redox systems[8−10,21−23] and especially the one dealing with the electron transfer across original W-shaped C_7 carbon-rich bridges *trans*-$[Cl(dppe)_2Ru{-}C{\equiv}C{-}C(CH_3){=}C(R^1){-}C(R^2){=}C{=}C{=}Ru(dppe)_2Cl](BF_4)$ (R^1 = Me, Ph, R^2 = H, Me),[9c] we decided to realize molecular wires with more than two metal centers using the $Ru(dppe)_2$ fragment. Such compounds will allow answering the fascinating question of whether these large size carbon-rich spacers can facilitate electron transfer over more than two metal centers of *the same type*, a priori preventing single electron trapping on one part of the structure. Herein, we report for the first time a complete study including (i) the synthesis of innovative highly conjugated complexes with three similar metal centers spanned by two odd-numbered C_7 π-conjugated chains and displaying well-separated redox processes and (ii) the complete studies of the different oxidation states using a combination of spectroscopic (UV−vis−NIR−IR and EPR) and theoretical techniques. In particular, careful EPR spectroscopy experiments and DFT calculations, unprecedented for such extended systems, turned out to be particularly valuable tools. As a result, we could provide a picture of electronic communication along these 28 Å long molecular wires. We illustrate the remarkable alternatives observed in different oxidation and reduction processes, owing to a remarkable behavior involving the metal centers and the non-innocent carbon-rich ligands as parts of the redox system. The original topology of these molecules, enforced by the limited available (bimetallic) complexes including odd-numbered carbon chains,[24−27] was recently highlighted in a preliminary report.[28]

Results and Discussion

Synthesis of the Complexes. We previously found that the deprotonable ruthenium allenylidene complexes of the type *trans*-$[(dppe)_2(Cl)Ru{=}C{=}C{=}C(CH_2R^1)R^2](BF_4)$ react with the neutral diynyl compound *trans*-$[Cl(dppe)_2Ru{-}(C{\equiv}C)_2{-}SiMe_3]$ to lead to stable dark green crystals of *trans*-$[Cl(dppe)_2Ru{-}C{\equiv}C{-}C(CH_3){=}C(R^1){-}C(R^2){=}C{=}C{=}Ru(dppe)_2Cl](BF_4)$ (R^1 = Me, Ph, R^2 = H, Me).[9c] In order to obtain the set of the trimetallic complexes [**3a**−**e**]$(OTf)_2$ bearing dppe and/or dppm diphosphine ligands (dppm =1,2-bis(diphenylphosphino)methane), we attempted the same type of reaction from the *trans* bis-diyne complexes **1a**,**b** and from 2 equiv of a metal allenylidene [**2a**−**c**](OTf) (Scheme 1). Slow addition over a period of several days led to clean stable blue-green solids of triruthenium complexes only in the cases of [**3a**,**b**]$(OTf)_2$ in 52% and 57% yield, respectively. For reasons that are still unclear so far, the reactions leading to [**3c**−**e**]$(OTf)_2$ proceeded in very low yields. Those three compounds were unambiguously indentified from HR-MS and ^{31}P NMR spectroscopies but could not be separated

(14) (a) Shan, N. S.; Vickers, J.; Adams, H.; Ward, M. D.; Thomas, J. A. *Angew. Chem., Int. Ed.* **2004**, *43*, 3938–3941. (b) Shan, N.; Ingram, J. D.; Easun, T. L.; Vickers, S. J.; Adams, H.; Ward, M. D.; Thomas, J. A. *Dalton Trans.* **2006**, 2900–2906.

(15) (a) Von Kamegke, A.; Tom, G. M.; Taube, H. *Inorg. Chem.* **1978**, *17*, 1790–1796. (b) Powers, M. J.; Callahan, R. W.; Salmon, D. J.; Meyer, T. J. *Inorg. Chem.* **1976**, *15*, 894–900.

(16) D'Alessandro, D. M.; Keene, F. R. *Dalton Trans.* **2006**, 1060–1072.

(17) For examples, see: (a) Bignozzi, C. A.; Paradini, C.; Roffia, S.; Scandola, F. *Inorg. Chem.* **1988**, *27*, 408–414. (b) Bignozzi, C. A.; Roffia, S.; Chiorboli, C.; Davilla, J.; Indelli, M. T.; Scansola, F. *Inorg. Chem.* **1989**, *29*, 4350–4358. (c) Geiss, A.; Kolm, M. J.; Janiak, C.; Vahrenkamp, H. *Inorg. Chem.* **2000**, *39*, 4037–4043. (d) Pfennig, B. W.; Fritchman, V. A.; Hayman, K. A. *Inorg. Chem.* **2001**, *40*, 255–263. (e) De Candia, A. G.; Singh, P.; Kaim, W.; Slep, L. D. *Inorg. Chem.* **2009**, *48*, 565–573.

(18) (a) Brown, G. M.; Mayer, T. J.; Cowan, D. O.; LeVanda, C.; Kafman, F.; Roling, P. V.; Rausch, M. D. *Inorg. Chem.* **1978**, *14*, 506–511. (b) Hore, L.-A.; MacAdam, C. J.; Kerr, J. L.; Duffy, N. W.; Robinson, B. H.; Simpson, J. *Organometallics* **2000**, *19*, 5039–5048. (c) Dong, T.-Y.; Chang, S.-W.; Lin, S.-F.; Lin, M.-C.; Sheng, Y.-S.; Lee, L. *Organometallics* **2006**, *25*, 2018–2024. (d) Lohan, M.; Ecorchard, P.; Rüffer, T.; Justaud, F.; Lapinte, C.; Lang, H. *Organometallics* **2009**, *28*, 1878–1890. (e) Bruce, M. I.; Low, P. J.; Hartl, F.; Humphrey, P. A.; de Montigny, F.; Jevric, M.; Lapinte, C.; Perkins, G. J.; Roberts, R. L.; Skelton, B. W.; White, A. H. *Organometallics* **2005**, *24*, 5241–5255. (f) Fan, Y.; Po-Chun, I.; Fanwick, P. E.; Ren, T. *Organometallics* **2009**, *28*, 3959–3962.

(19) (a) Yip, J. H.; Wu, J.; Wong, K.-Y.; Ho, K. P.; Pun, C. S.-N.; Vittal, J. J. *Organometallics* **2002**, *21*, 5292–5300. (b) Berry, J. F.; Cotton, F. A.; Murillo, C. A. *Organometallics* **2004**, *23*, 2503–2506. (c) Wong, W.-Y.; Lu, G.-L.; Ng, K.-H.; Choi, K.-H.; Lin, Z. *Dalton Trans.* **2001**, 3250–3260. (d) Kuo, C.-K.; Chang, J.-C.; Yeh, C.-Y.; Lee, G.-H.; Wang, C.-C.; Peng, S.-M. *Dalton Trans* **2005**, 3696–3701. (e) Sheng, T.; Varenkamp, H. *Eur. J. Inorg. Chem.* **2004**, 1198–1203. (f) Dewhurst, R. D.; Hill, A. F; Willis, A. C. *Organometallics* **2004**, *23*, 1646–1648. (g) Zuo, J. L.; Herdtweck, E.; de Biane, F. F.; Santos, A. M.; Kühn, F. E. *New J. Chem.* **2002**, *26*, 883–888. (h) Lin, Y.-C.; Chen, W.-T.; Tai, J.; Su, D.; Huang, S.-Y.; Lin, I.; Lin, J.-L.; Lee, M. M.; Chio, M. F.; Liu, Y.-H.; Kwan, K. S.; Chen, Y.-J.; Chen, H.-Y. *Inorg. Chem.* **2009**, *48*, 1857–1970. (i) Albinati, A.; Fabrizi de Biani, F.; Leoni, P.; Marchetti, L.; Pasquali, M.; Rizzato, S.; Zanello, P. *Angew. Chem., Int. Ed.* **2005**, *44*, 5702–5705.

(20) (a) Xu, G.-L.; De Rosa, M. C.; Crutchley, R. J.; Ren, T. *J. Am. Chem. Soc.* **2004**, *126*, 3728–3729. (b) Xu, G.-L.; Crutchley, R. J.; DeRosa, M. C.; Pan, Q.-J.; Zhang, H.-X.; Wang, X.; Ren, T. *J. Am. Chem. Soc.* **2005**, *127*, 13354–13363. (c) Zhu, Y.; Clot, O.; Wolf, M. O.; Yap, G. P.A *J. Am. Chem. Soc.* **1998**, *120*, 1812. (d) Lebreton, C.; Touchard, D.; Le Pichon, L.; Daridor, A.; Toupet, L.; Dixneuf, P. H. *Inorg. Chim. Acta* **1998**, *272*, 188. (e) Colbert, M. C. B.; Lewis, J.; Raithby, P. R.; White, J. P.; Williams, D. J. *Dalton Trans.* **1997**, 99–104.

(21) Rigaut, S.; Costuas, K.; Touchard, D.; Saillard, J.-Y.; Golhen, S.; Dixneuf, P. H. *J. Am. Chem. Soc.* **2004**, *126*, 4072.

(22) (a) Klein, A; Lavastre, O.; Fiedler, J. *Organometallics* **2006**, *25*, 635–643. (b) Ying, J.-W.; Liu, I. P.-C.; Xi, B.; Song, Y.; Campana, C.; Zuo, J.-L.; Ren, T. *Angew. Chem., Int. Ed.* **2010**, *49*, 954–957.

(23) (a) Fillaut, J.-L.; Andries, J.; Perruchon, J.; Desvergne, J.-P.; Toupet, L.; Fadel, L.; Zouchoune, B.; Saillard, J.-Y. *Inorg. Chem.* **2007**, *46*, 5922–5932. (b) Samoc, M.; Gauthier, N.; Cifuentes, M. P.; Paul, F.; Lapinte, C.; Humphrey, M. G. *Angew. Chem., Int. Ed.* **2006**, *45*, 7376–7379.

(24) (a) Bartik, T.; Johnson, M. T.; Arif, A. M.; Gladysz, J. A. *Organometallics* **1995**, *14*, 889–897. (b) Leroux, F.; Stumph, R.; Fischer, H. *Eur. J. Inorg. Chem.* **1998**, 1225–1234. (c) Kolokova, N. Y.; Skripkin, V. V.; Alexandrov, G. G.; Struchkov, Y. T. *J. Organomet. Chem.* **1979**, *169*, 293–300. (d) Weng, W. J.; Berenguer, R.; Fornies, J.; Lalind, E.; Martinez, F.; Sanchez, L.; Serrano, B. *Organometallics* **1998**, *17*, 1640–1642. (e) Bullock, R. M. *J. Am. Chem. Soc.* **1987**, *109*, 8087–8089. (f) Roth, G.; Reindl, D.; Gockel, M.; Troll, C.; Fischer, H. *Organometallics* **1998**, *17*, 1393–1401.

(25) (a) Bartik, T.; Weng, W.; Ramsden, J. A.; Szafert, S.; Falloon, S. B.; Arif, A. M.; Gladysz, J. A. *J. Am. Chem. Soc.* **1998**, *120*, 11071–11081. (b) Dembinski, R.; Szafert, S.; Haquette, P.; Lis, T.; Gladysz, J. A. *Organometallics* **1999**, *18*, 5438–5440. (c) Fuss, B.; Dede, M.; Weibert, B.; Fischer, H. *Organometallics* **2002**, *21*, 4425–4431.

(26) (a) Jia, G.; Xia, H. P.; Wu, W. F.; Ng, W. S. *Organometallics* **1997**, *16*, 2940–2947. (b) Xia, H. P.; Ng, W. S.; Ye, J. S.; Li, X. Y.; Wong, W. T.; Lin, Z.; Yang, C.; Jia, G. *Organometallics* **1999**, *18*, 4552–4557. (c) Selegue, J. P. *J. Am. Chem. Soc.* **1983**, *105*, 5921–5923. (d) Jimenez Tenorio, M. A.; Jimenez Tenorio, M.; Puerta, M. C.; Velerga, P. *Organometallics* **1997**, *16*, 5528–5535.

(27) (a) Antonova, A. B.; Bruce, M. I.; Ellis, B. G.; Gaudio, M.; Humphrey, P. A.; Jevric, M.; Melino, G.; Nicholson, B. K.; Perkins, G. J.; Skelton, B. W.; Stapleton, B.; White, A. H.; Zaitseva, N. N. *Chem. Commun.* **2004**, 960–961. (b) Bruce, M. I.; Ellis, B. G.; Skelton, B. W.; White, A. H. *J. Organomet. Chem.* **2005**, *690*, 1772–1783. (c) Hartbaum, C.; Fischer, H. *J. Organomet. Chem.* **1999**, *578*, 186–192.

(28) Olivier, C.; Choua, S.; Turek, P.; Touchard, D.; Rigaut, S. *Chem. Commun.* **2007**, 3100–3102.

Scheme 1. Synthesis of the Trimetallic Complexes

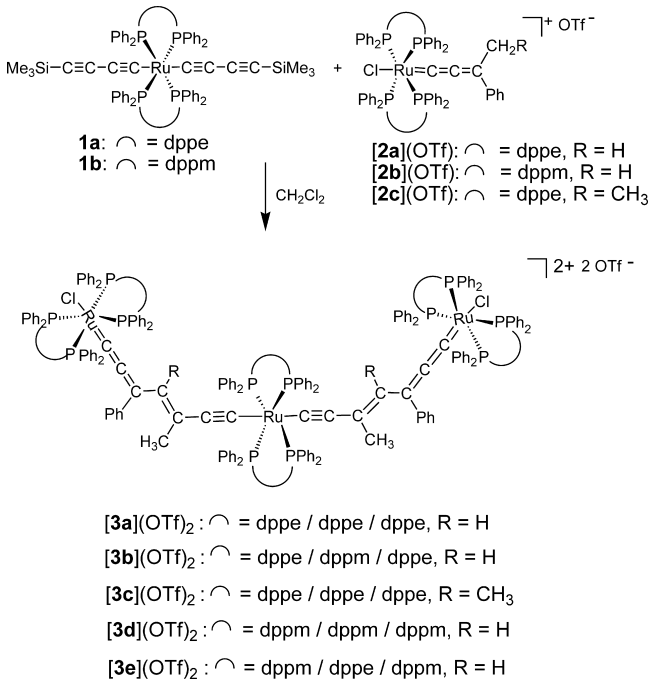

from the reaction mixture. Therefore, we chose to concentrate our efforts only on [**3a**,**b**](OTf)$_2$. As characteristic features for [**3a**](OTf)$_2$ as an example, the ^{1}H NMR spectrum presents one single signal for the methyl groups and one for the protons on the two chains at $\delta = 0.89$ and 5.76 ppm, respectively, characteristic of a symmetrical structure. The ^{31}P NMR analysis shows one singlet for the four equivalent phosphorus atoms of the central metal unit in *trans* arrangement ($\delta = 51.6$ ppm) and another singlet for those of the two identical remote metallic centers ($\delta = 44.9$ ppm). These signals are respectively closer to those of the bis-acetylide and of the allenylidene precursors than those of the bimetallic analogue [Cl(dppe)$_2$Ru−C≡C−C(CH$_3$)=CH−C(Ph)=C=C=Ru(dppe)$_2$Cl](OTf) [**4**](OTf).[9c] The ^{13}C NMR spectrum displays one set of seven different signals for the seven carbon atoms of the two symmetrical chains, assigned with the help of 2D HMBC and 2D HMQC experiments. The C_α resonance on the chain-end metal centers ($\delta = 260.6$ ppm) presents a higher allenylidene character than the two different carbenic carbons of the analogous bimetallic C_7 complex [**4**](OTf) displaying resonances at 230.2 and 224.0 ppm but is still upfield from that of the true allenylidene [**2a**](OTf) ($\delta = 310.6$ ppm). The other C_α resonance related to the central metal atom presents a signal at 193.0 ppm. Both observed signals are still downfield compared to that of **1a** (δ =131.8 ppm). Thus, NMR spectroscopies evidence a strong conjugation along the two identical carbon chains but, in contrast with [**4**](OTf), with a stronger weight for the mesomeric form displayed in Scheme 1 over the others (see Supporting Information). Not surprisingly, the cumulenic forms on the outside

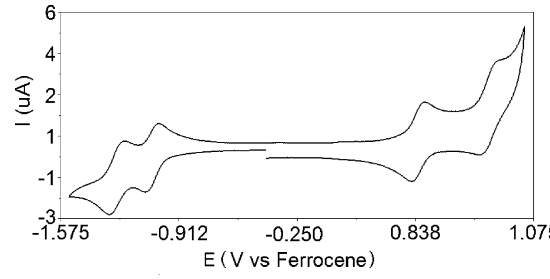

Figure 1. CV trace obtained for [**3a**]$^{2+}$ showing the two reduction and first two oxidation processes; Bu_4NPF_6 (0.2 M) in CH_2Cl_2; $\upsilon = 100$ mV·s^{-1}.

phenyl moieties are more favorable than those on the methyl. It is worth noting that this stabilization seems to be crucial as no compound without a pendant phenyl group on the chains could be obtained, as was the case with bimetallic analogues.

A further 2D NOESY experiment performed on [**3a**](OTf)$_2$ allows the observation of two correlation peaks involving the ortho hydrogen atoms on the chain phenyl group with (i) the proton on the tertiary carbon atom of chain and (ii) the hydrogen atoms of the methyl group. No correlation is observed between this proton of the chains and those of the methyl group. Therefore, these observations are also in line with a main contribution of the mesomeric form displayed in Scheme 1 with an allowed rotation around the bond between the carbon atom bearing the phenyl groups and that bearing the single hydrogen atom, and the *E* configuration of the double bonds. Concerning the FTIR spectra, both compounds present an intense absorption around $\nu = 1880$ cm^{-1} characteristic of the cumulenic character of the chain and a weak absorption around $\nu = 1990$ cm^{-1}, according to [**4**](OTf).

Electrochemical Data. The redox behavior of the trimetallic complexes [**3a**,**b**](OTf)$_2$ was investigated by means of cyclic voltammetry (CV) in CH_2Cl_2 solutions (0.2 M Bu_4NPF_6). The values of the potentials for all compounds are reported in Table 1. A typical CV profile is displayed in Figure 1. Both complexes undergo two reversible one-electron reductions and three one-electron oxidation processes (Table 1), the first one being reversible for both complexes. The second oxidation wave is reversible for [**3a**]$^{2+}$ and only partially reversible for [**3b**]$^{2+}$; the third one is irreversible for both complexes (not shown) and will not be further considered. Peak separations and comproportionation constants ($K_c = \exp(\Delta E°F/RT)$) derived from wave separations indicate that all redox species gain considerable thermodynamic stabilization. This might be the result of electronic delocalization due to the nature of the bridging ligands and of the metal centers, keeping in mind that K_c is not a true indication of the electronic coupling strength.[29]

Theoretical Results. The [**3a**]$^{n+}$ series ($n = 0-4$) was investigated theoretically by means of density functional theory calculations (DFT). To reduce computational effort, the complexes were slightly simplified by replacing the phenyl groups of the dppe ligands by hydrogen atoms leading to diphosphi-

Table 1. Electrochemical Data (CV) for the Trimetallic Complexes[a]

	$E°$ (+/0) Red2 (V)	$E°$ (2+/+) Red1 (V)	K_c[b] Red1/Red2	$E°$ (3+/2+) Ox1 (V)	$E°$ (4+/3+) Ox2 (V)	$E°$ (5+/4+) Ox3 (V)	K_c[b] Ox1/Ox2
[**3a**]$^{2+}$	−1.26	−1.07	1.9×10^3	0.40	0.81	1.14[e]	1.1×10^7
[**3b**]$^{2+}$	−1.32	−1.13	4.1×10^3	0.34	0.82[c]	1.05[e]	1.0×10^7[d]

[a] Sample, 1 mM; Bu_4NPF_6 (0.2 M) in CH_2Cl_2; $\upsilon = 100$ mV·s^{-1}; Potential are reported in volts vs the ferrocene/ferrocenium couple as an internal standard. Reversible redox processes $\Delta E_p \approx 60$ mV, $I_{pc}/I_{pa} \approx 1$. [b] $K_c = \exp(\Delta E°F/RT)$, $T = 293$K. [c] E_{pa} of a partially reversible peak $\Delta E_p \approx 90$ mV, $I_{pc}/I_{pa} \approx 0.65$. [d] Calculated with $E_{1/2}$. [e] Peak potential of an irreversible process.

Table 2. Pertinent Optimized Bond Lengths (Å) and Angles (deg) for the Modeled Complexes of [**3a**-H]$^{n+}$, (n = 0−4)[a]

compd	Ru^a-Cl $Ru^{a\prime}-Cl$	Ru^a-P $Ru^{a\prime}-P$	Ru^a-C_1 $Ru^{a\prime}-C_1'$	C_1-C_2 $C_1'-C_2'$	C_2-C_3 $C_2'-C_3'$	C_3-C_4 $C_3'-C_4'$	C_4-C_5 $C_4'-C_5'$	C_5-C_6 $C_5'-C_6'$	C_6-C_7 $C_6'-C_7'$	C_7-Ru^b $C_7'-Ru^b$	Ru^b-P	$C_{Me}-C_5-C_5'-C_{Me}'$
[**3a**-H]$^{0/S}$	2.566	2.352	2.035	1.245	1.410	1.404	1.408	1.400	1.249	2.085	2.351	−50.6
	2.571	2.351	2.038	1.244	1.416	1.412	1.412	1.403	1.248	2.082		
[**3a**-H]$^{0/T}$	2.566	2.351	2.037	1.245	1.410	1.407	1.409	1.407	1.246	2.100	2.347	−66.7
	2.570	2.351	2.039	1.244	1.414	1.417	1.403	1.410	1.244	2.096		
[**3a**-H]$^{0/BS}$	2.566	2.351	2.037	1.245	1.410	1.407	1.409	1.406	1.246	2.100	2.347	−67.6
	2.568	2.351	2.039	1.244	1.415	1.418	1.403	1.410	1.245	2.096		
[**3a**-H]$^{+}$	2.542	2.364	2.001	1.251	1.397	1.409	1.407	1.401	1.247	2.080	2.358	−101.7
	2.546	2.360	2.009	1.248	1.399	1.418	1.402	1.403	1.246	2.081		
[**3a**-H]$^{2+}$	2.522	2.378	1.970	1.258	1.381	1.417	1.402	1.399	1.247	2.072	2.370	−61.5
	2.532	2.375	1.974	1.256	1.386	1.400	1.400	1.400	1.247	2.070		
[**3a**-H]$^{3+}$	2.500	2.397	1.952	1.263	1.383	1.421	1.403	1.398	1.249	2.061	2.383	−76.3
	2.503	2.394	1.957	1.262	1.386	1.426	1.403	1.398	1.250	2.058		
[**3a**-H]$^{4+/T}$	2.454	2.421	1.938	1.270	1.383	1.407	1.410	1.392	1.252	2.059	2.393	−67.7
	2.469	2.4 14	1.950	1.268	1.390	1.421	1.412	1.393	1.253	2.045		
[**3a**-H]$^{4+/BS}$	2.459	2.420	1.935	1.271	1.383	1.406	1.412	1.391	1.252	2.058	2.392	−71.9
	2.473	2.419	1.949	1.267	1.390	1.425	1.409	1.385	1.253	2.051		
[**4**-H]^{0}	2.564	2.348	2.039	1.245	1.412	1.412	1.405	1.411	1.244	2.034	2.354	
[**4**-H]$^{+}$	2.531	2.365	1.989	1.253	1.392	1.408	1.412	1.390	1.253	1.983	2.368	
[**4**-H]$^{2+}$	2.489	2.405	1.960	1.261	1.388	1.421	1.415	1.390	1.260	1.961	2.402	

[a] See Chart 1 for atom labeling. T = triplet spin state; BS = broken symmetry singlet spin state; S = diamagnetic singlet spin state. Corresponding calculated distances for $[Cl(dpe)_2Ru-C\equiv C-C(CH_3)=CH-C(Ph)=C=C=Ru(dpe)_2Cl]^{n+}$ [**4**-H]$^{n+}$ from ref 9c are given for comparison (n = 0−2).

Chart 1

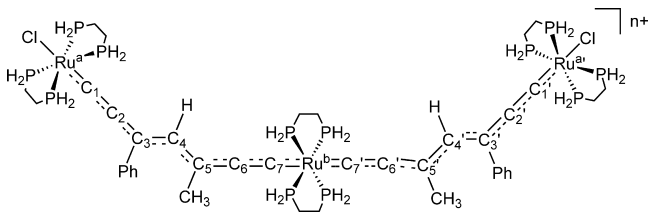

noethane ligands (dpe). Thus, the computed models are [**3a**-H]$^{n+}$ in the following. A full conformational analysis could not be envisaged because of a prohibitive computational cost. The choice of the conformation of the carbon bridges bearing three sp^2 carbon atoms was based on X-ray solid-state characterizations and on theoretical results previously obtained on the parent bimetallic complexes.[9c] In this earlier study, it was found that (i) the electronic structures were not notably affected by changes in the conformation of the carbon bridges,[30] (ii) the "W" shape of the bridge is one of the most stable, and (iii) the dipole moment of the latter is the highest of the series. Thus, it was concluded that the "W" shape should be one of the major conformations existing in polar solution. The "W" shape of the two bridges sketched in Scheme 1 was thus chosen for the present study of [**3a**-H]$^{n+}$ as a reference arrangement.

The main structural parameters of the resulting optimized geometries for the "W"-shaped chains are given in Table 2, and additional data are given in Table S4 in Supporting Information. They are compared to equivalent values of the related bimetallic systems [**4**-H]$^{n+}$ since no experimental X-ray characterization is available in the trimetallic series. Both external conjugated chains ($C_1^{(\prime)}$, $C_2^{(\prime)}$, $C_3^{(\prime)}$, see Chart 1) present metrical data very close to the distances calculated for the bimetallic parent [**4**-H]$^{+}$. In full agreement with the NMR data, their structural arrangements present a more important allenylidene character than the two inner parts linked to the middle ruthenium atom ($C_7^{(\prime)}$, $C_6^{(\prime)}$, $C_5^{(\prime)}$). Indeed, the average Ru−C bond in [**3a**-H]$^{n+}$ is 1.970 Å for the external ruthenium atoms, whereas it is calculated to be of 2.071 Å for the central ruthenium atom. The C−C bond lengths reveal also the increased allenylidene character of the outer part of the molecule. It has to be noted that the two chains are almost structurally identical.

The electronic structure of [**3a**-H]$^{2+}$ is described in Figure 2. At first sight, it can be described as a doubling of the electronic structure of the bimetallic [**4a**-H]$^{+}$.[9c] The HOMO−LUMO energy gap is large (1.29 eV). The first two LUMOs are well separated from the rest of the virtual orbitals by 1.15 eV. They can be depicted as the in-phase and out-of-phase combination of the LUMO of [**4a**-H]$^{+}$ (see Figure 2). The eight highest HOMOs can be similarly deduced for the four highest HOMOs of [**4a**-H]$^{+}$. They are delocalized over the conjugated skeleton, presenting an antibonding ruthenium−carbon and ruthenium−chlorine character. They are more confined on the external part of the molecule. On the contrary, the HOMO-4 and HOMO-5 are more localized on the central $C_6C_7-Ru^b-C_7'C_6'$ chain.

Before we discuss the general trends occurring upon the oxidation and reduction processes, it is worth mentioning that the di-oxidized and di-reduced systems, [**3a**-H]$^{4+}$ and [**3a**-H], can be found as triplet or singlet spin state compounds. Both were considered in the calculations. Taking into account the level of theory and of modeling, the differences in energy between the spin states can only be considered as approximate. The singlet state can be either a "conventional" closed-shell system with all electrons paired or a diradical one with the two magnetic electrons in distinct spin orbitals, antiferromagnetically coupled. The broken symmetry (BS)[31] density functional approach was shown to be efficient in evaluating the energy of the antiferromagnetic diradicalar singlet.[32] In both cases, [**3a**-H]$^{4+}$ and [**3a**-H], the BS singlet state was calculated to be lower in energy than the triplet state by 0.10 and 0.03 eV, respectively. The closed-shell structure is much higher in energy for [**3a**-H] (+0.24 eV).[33] In order to evaluate the magnetic coupling constant of [**3a**-H] and [**3a**-H]$^{4+}$, the procedure of Ruiz and colleagues was employed (see Computational Details).[34] The

(29) (a) Barrière, F.; Camire, N.; Geiger, W. E.; Mueller-Westerhoff, U. T.; Sanders, R. *J. Am. Chem. Soc.* **2002**, *124*, 7262–7263. (b) Lapinte, C. *J. Organomet. Chem.* **2008**, *693*, 793–801.

(30) With selected forms I, II, and III from Scheme S2 with X = Cl. Form IV is unstable for steric reasons.

(31) Noodleman, L. *J. Chem. Phys.* **1981**, *74*, 5737–5743.

(32) The best-suited methods (CASSCF or CI) for such calculations are still nowadays unaffordable in terms of computing time and memory.

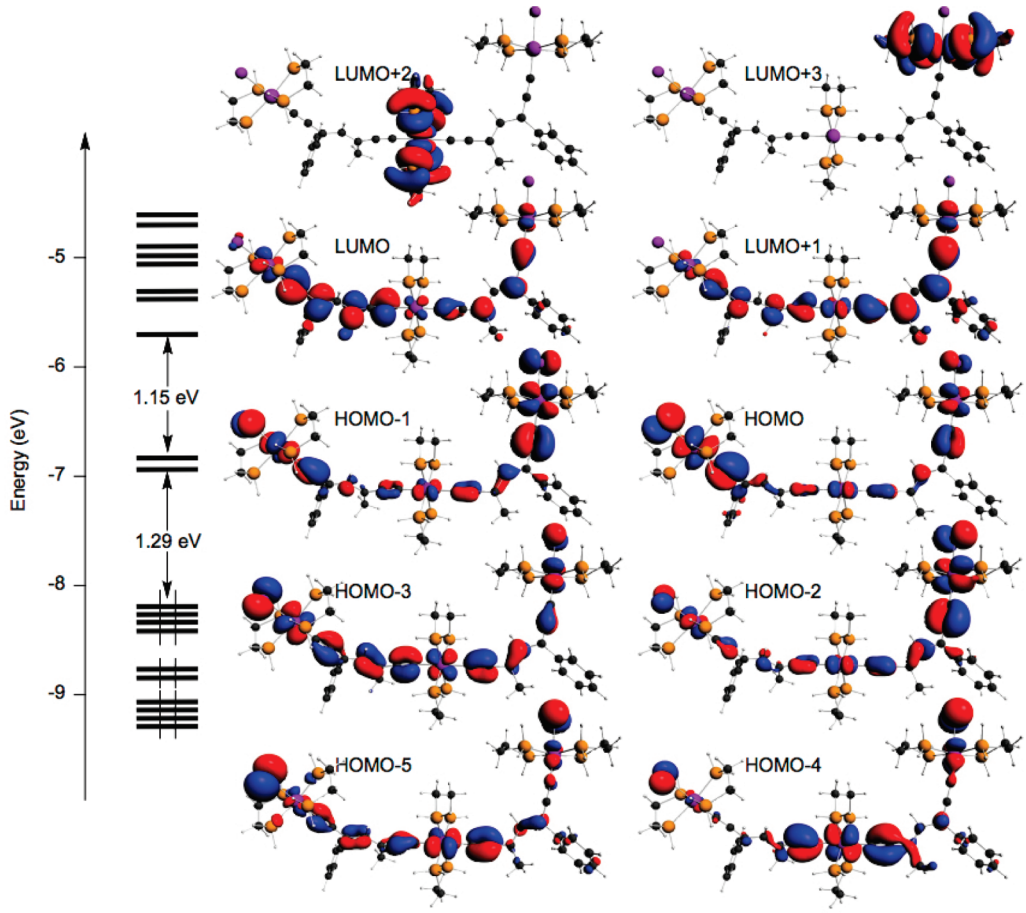

Figure 2. Molecular orbital diagram of [**3a**-H]$^{2+}$ in its optimized geometry with "W"-shaped chains. Iso-contours of the plotted orbitals = ±0.025 (e·bohr^{-3})$^{1/2}$.

calculated coupling J_{ab} is antiferromagnetic in each case and is calculated to be −0.022 eV for [**3a**-H] and −0.103 eV for [**3a**-H]$^{4+}$.

Concerning the two oxidation processes (n = 3, 4), they can be described roughly as the removal of electrons of the highest occupied molecular orbitals (HOMOs), inducing electronic and geometrical rearrangements. The main structural changes are observed in the distances between the external ruthenium atoms and their surrounding ligands. The Ru$^{a(\prime)}$−Cl and Ru$^{a(\prime)}$−C$_1^{(\prime)}$ bonds are shortened by roughly 0.03 and 0.01 Å upon one-electron oxidation, whereas the Ru$^{a(\prime)}$−P distances are lengthened by 0.02 Å. The central ruthenium atom is similarly affected but to a lesser extent (see Table 2). The changes calculated in the conjugated carbon bridges, even though they are small (less than 0.01 Å),[35] illustrate an evolution to a more cumulenic structure of the external parts, the central part being marginally affected upon oxidation. Upon reduction of [**3a**-H]$^{2+}$, the main geometrical rearrangements occur on the ClRu$^{a(\prime)}$(dpe)C$_1^{(\prime)}$=C$_2^{(\prime)}$=C$_3^{(\prime)}$(Ph) motifs, the rest of the molecule being much less affected. The two first LUMOs of [**3a**]$^{2+}$ are essentially nonbonding between the carbon atoms of the conjugated path, the C−C distances are thus hardly affected upon reduction. The main change in the carbon chains is a lengthening of ca. 0.01 Å for C$_2^{(\prime)}$−C$_3^{(\prime)}$ after the first and the second one-electron reductions.

The spin densities of [**3a**-H]$^{n+}$ (n = 0, 1, 3, 4) in a geometry with "W"-shaped chains are given in Table 3 and sketched in Figure 3. Overall, the unpaired electrons in the oxidized species are equally spread out over the ruthenium atoms and the carbon atoms of the conjugated path in that configuration. A noticeable atomic spin density is found on the terminal chlorine atoms. The reduced radical species present a strongly polarized spin density quasi-exclusively localized on the carbon atoms of the conjugated skeleton. The positive atomic spin density is mainly found on C$_1^{(\prime)}$, C$_3^{(\prime)}$, C$_5^{(\prime)}$, and C$_7^{(\prime)}$ (see Figure 3).

Several starting structural arrangements and guess densities were tested in order to evaluate the capacity of localization of the unpaired electron in monoreduced species [**3a**-H]$^{+}$. In each system considered, an asymmetrical guess density was chosen in order to allow the localization of the unpaired electron on one of the halves of the molecule. The geometrical arrangements investigated were carefully chosen on the basis of the previous theoretical study performed on [**4a**-H]$^{+}$ and on the basis of the experimental data. NMR results suggest for [**3a**](OTf)$_2$ that a free rotation is allowed around the C(H)−C(Ph) bonds of the conjugated bridge. Accordingly, our theoretical investigations on [**3a**-H]$^{+}$ show that while a rotation around the C(Me)−C(H) bond is too energetically demanding to occur (0.79 eV), a rotation around the C(H)−C(Ph) bond costs only 0.26 eV in

(33) In the case of [**3a**-H]$^{4+}$, the closed shell singlet state was not obtained due to SCF convergence problems. Most probably, this system would be much higher in energy than the BS and T states as found for [**3a**-H]^{0}.
(34) Ruiz, E.; Alvarez, S.; Cano, J.; Polo, V. *J. Chem. Phys.* **2005**, *123*, 164110.
(35) These differences in the distances are larger than the optimization criteria.

Table 3. Atomic Mulliken Spin Densities Calculated for the Modeled Complexes of [**3a**-H]$^{n+}$, for n = 0, 1, 3, 4[a]

compd	Cl Cl′	Ru[a] Ru[a′]	C_1 C_1'	C_2 C_2'	C_3 C_3'	C_4 C_4'	C_5 C_5'	C_6 C_6'	C_7 C_7'	Ru[b]
[**3a**-H]$^{0/T}$	−0.00	+0.03	+0.25	−0.09	+0.37	−0.14	+0.37	−0.09	+0.27	+0.03
	−0.00	+0.03	+0.25	−0.09	+0.36	−0.13	+0.33	−0.07	+0.23	
[**3a**-H]$^{0/BS}$	−0.00	+0.03	+0.25	−0.09	+0.36	−0.14	+0.37	−0.11	+0.27	+0.00
	+0.00	−0.03	−0.24	+0.08	−0.35	+0.13	−0.32	+0.09	−0.24	
[**3a**-H]$^{+}$	+0.00	+0.02	+0.13	−0.04	+0.18	−0.07	+0.19	−0.05	+0.13	+0.01
	+0.00	+0.02	+0.13	−0.04	+0.18	−0.07	+0.16	−0.04	+0.11	
[**3a**-H]$^{3+}$	+0.07	+0.18	+0.00	+0.13	−0.02	+0.04	−0.01	+0.05	+0.00	+0.10
	+0.06	+0.18	+0.00	+0.13	−0.03	+0.06	−0.02	+0.06	+0.01	
[**3a**-H]$^{4+/T}$	+0.16	+0.39	+0.02	+0.28	−0.04	+0.03	−0.02	+0.06	−0.01	−0.14
	+0.14	+0.38	+0.00	+0.26	−0.06	+0.12	−0.03	+0.01	+0.02	
[**3a**-H]$^{4+/BS}$	+0.15	+0.39	+0.02	+0.29	−0.03	+0.00	−0.00	−0.02	+0.00	−0.08
	−0.12	−0.35	−0.00	−0.24	+0.05	−0.10	+0.02	−0.06	−0.02	

[a] See Chart 1 for atom labeling. T = triplet spin state; BS = broken symmetry singlet spin state.

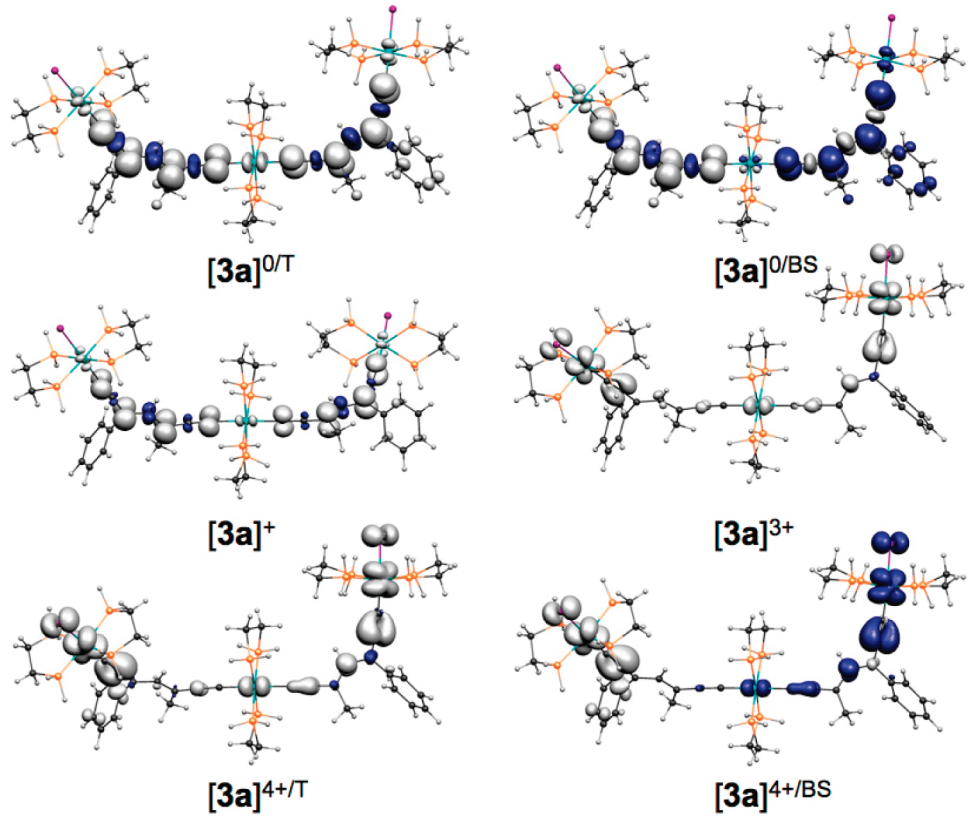

Figure 3. Spin densities calculated for the model complexes of [**3a**-H]$^{n+}$, for n = 0, 1, 3, 4. See Chart 1 for atom labeling. T = triplet spin state; BS = broken symmetry singlet spin state. Iso-contours = ±0.0025 e·bohr^{-3}.

vacuum (see Supporting Information). Thus, the optimization of this rotation leads to a cationic structure that corresponds to a conformation in which a rotation of nearly 90° is found along the $C_3'-C_4'$ bond, whereas it is of 0° in the arrangements with "W"-shaped chains. This arrangement leads to a partial localization of the unpaired electron on the C_1' and C_3' of 0.23 and 0.38, respectively, the rest of the spin density being found on the other (planar) carbon chain, and the central ruthenium atom has a slightly unsymmetrical arrangement (Ru−C_1 = 2.069 Å; Ru−C_1' = 2.104 Å).

A similar study was performed on the tricationic (singly oxidized) system [**3a**-H]$^{3+}$. The optimized geometry shows a torsion angle $C_5'-C_4'-C_3'-C$(Ph) of nearly 40°. The geometrical data are not drastically modified compared to the structure with "W"-shaped chains. The spin density is only slightly modified with a repartition of 0.18 (vs 0.19), 0.13 (vs 0.08), and 0.15 (vs 0.20) electrons on the Ru[a], Ru[b], and Ru[a′] atoms, respectively. Two other structural modifications were evaluated: the rotation of each Ru(dpe)$_2$ unit and the rotation of each "W" chain with respect to the other, starting from a geometry in which one chain has the same geometry as [**3a**-H]$^{2+}$ and the other one that of [**3a**-H]$^{0/T}$ or [**3a**-H]$^{4+/T}$. In the case of the monoreduced system [**3a**-H]$^{+}$, the spin density between the two chains can be rendered asymmetric up to roughly 20% (see Supporting Information). This conformation, slightly higher in energy than the fully delocalized ones, corresponds to a structure in which the chains are not equivalent, with on one hand the structural arrangement of the dicationic optimized geometry and on the other hand the one of the neutral high spin system, the two planes of the chain forming an angle of nearly 90°. On the other hand, in the case of the monooxidized system, the distances and spin density are hardly

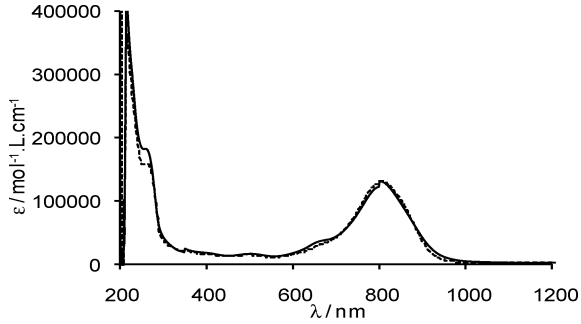

Figure 4. Electronic absorption spectra for [**3a**](OTf)$_2$ (solid) and [**3b**](OTf)$_2$ (dashed) in CH_2Cl_2.

affected and stay roughly symmetrical upon rotations. Nevertheless, the total energy changes within a range of ±0.35 eV. Although it was not possible to consider exhaustively all possible rotamers because of computational cost, these results strongly suggest that a localized structure is less favorable in the reduced species and unlikely in the oxidized one.

Finally, time-dependent DFT (TD-DFT) calculations were performed on [**3a**-H]$^{2+}$ in three different structural arrangements (see Table S5 and Figure S15 in Supporting Information). Each arrangement leads to distinct absorption spectra. The experimental measurements (*vide infra*) can thus be seen as the superposition of individual geometrical structures. Indeed, the oscillator strengths are calculated to be actually different depending on the structural arrangement for symmetry reasons. A global description can nevertheless be drawn. Excitations between 900 and 500 nm are described as combinations of transitions between orbitals from the HOMO-5/HOMO block to the LUMO and LUMO+1 orbitals. The experimental absorption band found at low energy (Figure 4) can thus be described as a ClRu(d)-bridge(π) to bridge(π^*) charge transfer. On the other hand, the band at ca. 500 nm can be assigned to a ligand to ligand charge transfer ($\pi \rightarrow \pi^*$) mainly due to HOMO-6/HOMO-9 to LUMO/LUMO+1 transitions. It is worth noting that TD-DFT calculations on open shell systems are known to lead to unphysical transitions and thus were not handled in this system particularly sensitive to spin-contamination.[36]

UV−vis Spectra. As depicted in Figure 4, in addition to the classical intense short-wavelength absorption bands originating from the dppe/dppm ligands at high energy below 300 nm, the deep blue-green solutions of both complexes in CH_2Cl_2 display a broad band with a large extinction coefficient obviously composed of several transitions (Table 4). As suggested by the MO diagrams and the TD-DFT calculations detailed above, this experimental band is in fact the result of the superposition of the absorption of individual geometrical structures that displays several closely related transitions with mainly a metal-to-ligand charge transfer (MLCT) character. It is of note that they are not influenced by the nature of the central phosphines. The presence of a third metallic center has the effect of increasing the absorptivity and shifting the transition to lower energy relative to the bimetallic congener ($\lambda_{max} = 764$ nm, $\varepsilon = 98\,000$ M^{-1} cm^{-1}), which is indicative of a longer conjugated path in the ground state through the central metal atom. Accordingly, the energy gap between the occupied orbitals and the vacant orbitals is found smaller for the π-extended complex [**3a**-H]$^{2+}$ (*vide supra*) than for [**4a**-H]$^+$ (1.3 vs 1.4 eV).

Studies of the Oxidized and Reduced Species. To collect more detailed experimental information about oxidized and reduced species, i.e., to assess the electronic configuration in each redox state and therefore the electronic communication taking place within these species, a series of spectroscopic experiments covering the IR, NIR, visible, and UV regions of the spectrum as well as EPR studies were performed on in situ chemically or electrochemically generated samples.

EPR Spectroscopy. The EPR properties of the paramagnetic trications [**3a**]$^{3+}$ and [**3b**]$^{3+}$ (mono oxidized species) were obtained *via in situ* electrolysis in CH_2Cl_2/0.1 M Bu_4NPF_6 at 77 K and at 4 K. Although almost isotropic at 77 K, a small distortion of the EPR signal of [**3b**]$^{3+}$ is observed at 4 K (Figure 5), yielding a slightly anisotropic rhombic *g*-tensor (Table 5).[28] The EPR spectrum of [**3a**]$^{3+}$ is almost fully isotropic and centered at $g = 2.0047$ at 77 K, while being slightly asymmetrical and shifted to higher field with an average *g*-value close to 2.001 at 4 K (see Supporting Information). It has been much used as an empirical rule that the principal values of the *g*-tensor may be considered as a qualitative estimation of the extent of the electron over the metal and/or over the ligand upon checking the departure from the free electron *g*-value.[37] Accordingly, small *g* anisotropy and an average <*g*> factor not strongly shifted compared to the free electron *g*-value, g_e, suggest a dominant π-orbital character of the single electron orbital being characteristic of metal stabilized but highly ligand centered paramagnetic species. Such a behavior is observed for the whole series of [**3a**]$^{n+}$ and [**3b**]$^{n+}$ derivatives, the *g*-tensor of both derivatives being assessed as isotropic or slightly anisotropic for such Ru derivative.[9c,37] This is further supported by the present DFT calculations performed for [**3a**-H]$^{n+}$ ($n = 0-4$), see Table 3, which show the large delocalization of the spin density over the conjugated ligand. It is worth noting that recent work[38] could give some insight in the discussion of the *g*-tensor of ruthenium arylacetylide derivatives, pointing toward the fact that the anisotropy of the *g*-tensor cannot solely account for the detailed spin distribution over the molecule. This is shown in the present work, since calculated Ru spin densities emphasize the increasing role of the side Ru$^{a(')}$ atoms with respect to the central Ru^b atom when going from $n = 1$ to 4, whereas the EPR *g*-tensor does not show sensitivity to such a spin distribution.[39]

Setting the oxidation potential to the second peak of the CV and cooling the solution to 4 K yielded a weak EPR signal for [**3a**]$^{4+}$ and [**3b**]$^{4+}$, the features of which are very similar to those observed for [**3a**]$^{3+}$ and [**3b**]$^{3+}$ (Figure S1 in Supporting Information). The temperature dependence of the EPR response was investigated between 4 and 100 K. Since the shape of the signal does not change with temperature, the EPR susceptibility is estimated by the peak-to-peak amplitude, A_{pp}, of the EPR

(36) Casida, M. E.; Ipatov, A.; Cordova, F. In *Time-Dependent Density Functional Theory*; Marques, M. A. L., Ullrich, C., Nogueira, F., Rubio, A., Gross, E. K. U. Eds.; Springer: Berlin, 2006.

(37) (a) Kaim, W.; Ernst, S.; Kasack, V. *J. Am. Chem. Soc.* **1990**, *112*, 173–178. (b) Kasack, V.; Kaim, W.; Binder, H.; Jordanov, J.; Roth, E. *Inorg. Chem.* **1995**, *34*, 1924–1933. (c) Patra, S.; Sarkar, B.; Ghumaan, S; Fiedler, J.; Kaim, W.; Lahiri, G. K. *Dalton Trans.* **2004**, 754–758.

(38) Gauthier, N.; Tchouar, N.; Justaud, F.; Argouarch, G.; Cifuentes, M. P.; Toupet, L.; Touchard, D.; Halet, J.-F.; Rigaut, S.; Humphrey, M. G.; Costuas, K.; Paul, F. *Organometallics* **2009**, *28*, 2253–2266.

(39) A possible explanation is that the experimental *g*-tensor obviously does not probe separately the spin-orbit contribution of the three Ru atoms and the all conformations. The EPR response averages these contributions over the whole molecule, and the dominant mechanism is the delocalization leaving the average *g*-tensor almost isotropic and close to $g = 2$.

Table 4. UV−vis and NIR Data for [**3a**,**b**]$^{n+}$ ($n = 0-4$) in CH_2Cl_2

	UV−vis[a]		NIR[a]	
	λ_{max}, nm (ε, $mol^{-1} \cdot L \cdot cm^{-1}$)	λ_{max}, nm/ν_{max}, cm^{-1} (ε, $mol^{-1} \cdot L \cdot cm^{-1}$)	$\Delta\nu_{1/2}$, cm^{-1}	$\Delta\nu_{1/2}$ (calcd)[b], cm^{-1}
[**3a**]$^{4+}$	798 (40 200), 656 (41 700)	1728/5787 (5860)	2560	
[**3a**]$^{3+}$	800 (126 000), 682 (sh), 506 (22 300)	1378/7257 (3850)	3380	
[**3a**]$^{2+}$	802 (147 000), 682 (sh), 504 (20 100)			
[**3a**]$^{+}$	800 (40 300), 960 (10 300)	2630/3800 (4400)	3070	2962
3a	broad in all of the vis range (∼25 000)			
[**3b**]$^{4+}$	800 (55 000), 682 (37 600)	1656/6040 (6590)	2300	
[**3b**]$^{3+}$	800 (122 000), 688 (sh), 496 (14 600)	1300/7788 (995)	3640	
[**3b**]$^{2+}$	800 (130 000), 688 (sh), 498 (13 600)			
[**3b**]$^{+}$	780 (61 000), 948 (11 300)	ca. 2500/4000 (5000) br.	ca. 3500	ca. 3000
3b	broad in all of the vis range (∼25 000)			

[a] In CH_2Cl_2. [b] Calculated from $\Delta\nu_{1/2} = (2310\nu_{max})^{1/2}$ for symmetrical systems.

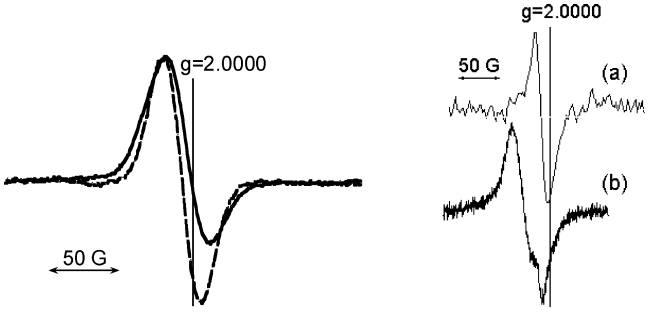

Figure 5. First derivative EPR spectra recorded at 77 K (dashed line) and at 4 K (solid line) in CH_2Cl_2 frozen solution for [**3a**]$^{3+}$ (left) and [**3b**]$^{3+}$ (right).

Table 5. *g*-Tensors of the Different Ionic Species Generated through Electrolysis Experiments and Potassium Mirror Reduction Experiments at 4 K[a]

	g_1	g_2	g_3	g_{iso}
[**3a**]$^{3+}$				2.0047[b]
[**3b**]$^{3+}$	2.0265[b]	2.016[b]	2.0015[b]	<2.0147>
[**3a**]$^{+}$				2.004[c]
[**3b**]$^{+}$				2.006[c]
3a				2.0052[c]
3b				2.0085[c]

[a] The g_{iso} value is given at room temperature for **3a** and **3b**, and at 4 K for other ions. Value within brackets corresponds to the average of the principal values of the *g*-tensor at 4 K. [b] Electrolysis experiments. [c] Potassium mirror reduction experiments.

signal (first derivative of the absorption). The plot of the reciprocal EPR susceptibility vs temperature roughly affords a Curie-like behavior (see Supporting Information). Therefore, it is suggested that the two-electron oxidation of both compounds is EPR-silent, and the observed noisy spectra (Figure S1) correspond to a small fraction of the singly oxidized compounds. This is most probably caused by a singlet−triplet gap $\Delta E_{S\text{-}T}$ much larger than kT, so that the monocation is solely observed as a doublet spin impurity. This is corroborated by the DFT calculations of the S/T gap assessing the value of a few kT for [**3a**-H]$^{4+}$ with the BS singlet state being the ground state. Accordingly, no detectable EPR signal is expected below ca. 100 K for an S/T gap larger than, e.g., 4 kT. This is in line with the conclusions drawn for bis-ruthenium dicationic derivatives involving cumulenic resonance.[40]

As the electrolytic route ends up with a poor S/N ratio, the addition of successive electrons was achieved by reduction on a potassium mirror. This was performed, while checking online the EPR and UV−vis absorption spectra of the solution (*vide infra*). After a short contact with the potassium mirror, an EPR

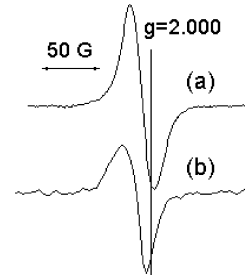

Figure 6. EPR spectra in THF solution and at room temperature of the monocations (a) [**3a**]$^{+}$ and (b) [**3b**]$^{+}$.

spectrum is observed at room temperature that consists of a single line ($\Delta H_{pp} = 20$ G and $g = 2.0040$ for [**3a**]$^{+}$ and $\Delta H_{pp} = 15$ G and $g = 2.0060$ for [**3b**]$^{+}$) without hyperfine structure (Figure 6).

The frozen solution shows EPR features quite identical for both complexes and the related anisotropic *g*-values ($<g> = 2.0050$) are consistent with a ligand centered paramagnetic species (see Supporting Information). The first reduction of the complexes leads to the same EPR spectra at 4 K as those observed after electrolysis generation. It has been checked that the intensity of the EPR signal decreases as the temperature increases, as expected for a Curie law with doublet ($S = 1/2$) spins.

When extending the contact of the solution with the potassium mirror, the UV−vis spectrum of the solution confirms the obtaining of the neutral species **3a** and **3b**. Whereas at room temperature the EPR spectrum of **3a** exhibits an almost symmetrical single line ($\Delta H_{pp} = 13.8$ G), **3b** shows some resolved splitting attributed to hyperfine couplings, and it is centered at $g = 2.0085$ with a similar spectral width (Figure 7). However, because of the lack of well resolved structure of the recorded spectrum that implies hidden information, it was not possible to assign the observed couplings. For instance, *at least* two sets with different numbers of nuclei and hfcc's could reproduce the experimental EPR spectra (see Supporting Information). None of these possible sets can be reasonably related to previous assignments for a related bimetallic Ru-based monoradical [**4a**]$^{\bullet}$.[9c,41] Last, attempts to perform ENDOR experiments have failed.

In frozen solution, the EPR spectra of **3a** and of **3b** are very similar, with a single and slightly distorted line (see Supporting

(40) (a) Bruce, M. I.; Elis, B. G.; Low, P. J.; Skelton, B. W.; White, A. H. *Organometallic* **2003**, *22*, 3184–3198. (b) Bruce, M. I.; Costuas, K.; Davin, T.; Ellis, B. G.; Halet, J.-F.; Lapinte, C.; Low, P. J.; Smith, M. E.; Skelton, B. W.; Toupet, L.; White, A. H. *Organometallic* **2005**, *24*, 3864–3881.

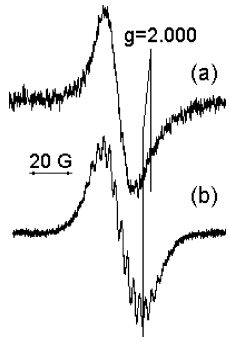

Figure 7. Room temperature EPR spectrum of the neutral species THF solutions (a) **3a** and (b) **3b**.

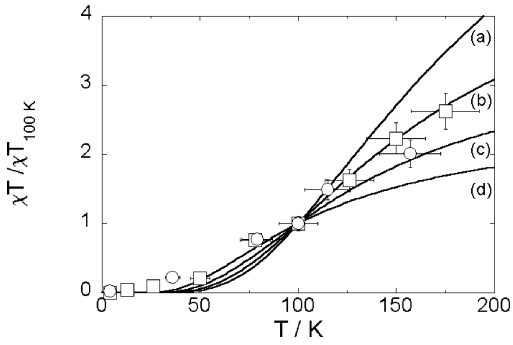

Figure 8. Temperature dependence of the product $A_{pp}T$ for **3a** (open squares) and **3b** (open circles). Values are normalized to the value at 100 K in order to compare relative values with the theoretical expectations. The solid lines represent the theoretical Bleaney−Bowers law for a singlet−triplet equilibrium with $\Delta E_{ST}/k = 350$ K (a), 300 K (b), 250 K (c), and 200 K (d).

Information). Although rather weak signals were obtained, especially in the case of **3a**, their temperature dependence has been estimated in an attempt to get the magnetic ground state of these neutral species. It is depicted by the χT plot of the EPR intensity represented by $A_{pp}T$ vs T (Figure 8). The generation of the neutral species is corroborated by the fact that the EPR intensity no longer obeys a Curie law, since it obviously decreases as the temperature decreases, thus pointing toward a diamagnetic singlet ($S = 0$) ground state. Despite the large uncertainties, the thermal magnetic behavior may be approximated by the expected Bleaney−Bowers law for singlet−triplet equilibrium ($\chi T = (3C)/(3 + \exp(-\Delta E_{ST}/kT))$), with ΔE_{ST} the singlet−triplet gap, and C the Curie constant for two doublet spins. It is concluded that (i) the two derivatives have a similar behavior, and (ii) the singlet−triplet gap is of the order of room temperature, in very good agreement with the DFT calculations yielding an S/T gap of the order of kT for **3a**-H, i.e., 0.255 eV, and pointing to a diradicaloïd character

To conclude this section, it is interesting to note that the g-tensor in $[\mathbf{3a}]^{n+}$ is almost fully isotropic, whereas that of $[\mathbf{3b}]^{n+}$ is found to be anisotropic, the difference between the two systems being the chelating phosphines on the central Ru atom (dppe vs dppm, respectively). This slight difference is not unexpected since a change in the bite angle of the diphosphine ligands generates a different degeneracy splitting in the pseudo-t_{2g} set of orbitals, the latter being directly correlated to the EPR anisotropy.[38] It is worth emphasizing the sensitivity of EPR to

(41) Note that this compound may be considered as a fragment, being half of **3b** bearing dppm ligands on the central ruthenium atom instead of dppe.

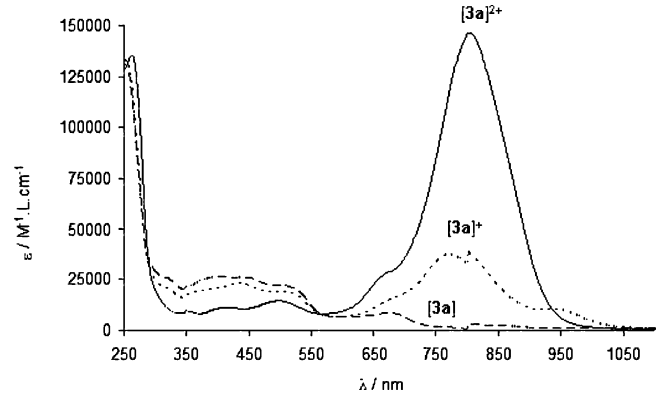

Figure 9. Electronic absorption spectra obtained upon the first and the second reduction of $[\mathbf{3a}]^{2+}$ in an OTTLE cell (CH_2Cl_2, 0.2 M Bu_4NPF_6).

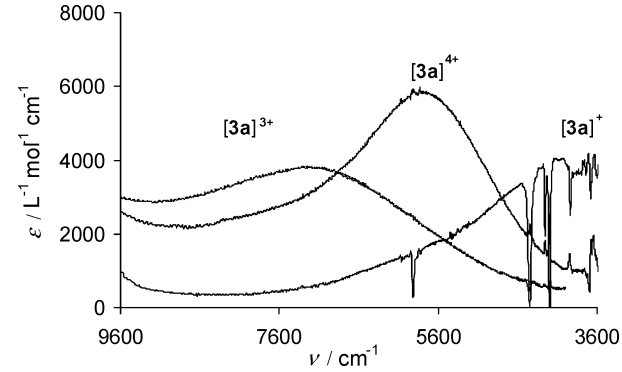

Figure 10. Difference spectra obtained in the NIR region for $[\mathbf{3a}]^{3+}$, $[\mathbf{3a}]^{4+}$, and $[\mathbf{3a}]^{+}$ in CH_2Cl_2 (0.2 M Bu_4NPF_6).

probe quite slight modifications of the electronic distribution between two closely related molecules.

UV−vis/NIR/IR Spectroelectrochemical Experiments. The optical properties of $[\mathbf{3a},\mathbf{b}]^{n+}$ ($n = 0-4$) were investigated by means of UV−vis/NIR spectroelectrochemistry in an OTTLE cell. Both species show similar behaviors (Table 4). As an example, upon the first one-electron reduction of $[\mathbf{3a}]^{2+}$ to $[\mathbf{3a}]^{+}$, the intense absorption decreases and shifts to slightly higher energy (Figure 9, for $[\mathbf{3b}]^{n+}$ see Supporting Information).[42] Upon further reduction to **3a**, the discoloration of the mixture and thus the vanishing of the intense visible bands were observed as was the case with the bimetallic analogues. A simplistic speculative explanation based on the hypothesis of small geometrical and electronic relaxations is that these observations would result from the sequential additions of electrons in the π^* orbitals of the conjugated ligand and thus in a decrease of the transition probabilities from deeper levels (Figure S15 in Supporting Information). Upon the first one-electron reduction, a new broad band shows up in the NIR region (Figure 10) and collapses on further reduction to **3a**. IR monitoring of the first reduction of $[\mathbf{3a}]^{2+}$ ($[\mathbf{3b}]^{2+}$) to $[\mathbf{3a}]^{+}$ ($[\mathbf{3b}]^{+}$) shows the vanishing of the vibration of $[\mathbf{3a}]^{2+}$ ($[\mathbf{3b}]^{2+}$) at 1990 cm^{-1} (1994 cm^{-1}), a slight shift of the characteristic vibration stretch from 1880 cm^{-1} (1890 cm^{-1}) to 1902 cm^{-1} (1913 cm^{-1}), and a new broad band between 1850 and 1700 cm^{-1} centered at 1794 cm^{-1} (1805 cm^{-1}) (Figure 11). Further vanishing of all bands is observed

(42) (a) We assume that all of the complex is reduced to $[\mathbf{3a}]^{+}$ in the solution. Quantitative prediction leads to a theoretical composition of 98% of $[\mathbf{3a}]^{+}$ with $\Delta E^{\circ} = 190$ mV, see ref b. (b) Connelly, N. G.; Geiger, W. E. *Chem. Rev.* **1996**, *96*, 877–910.

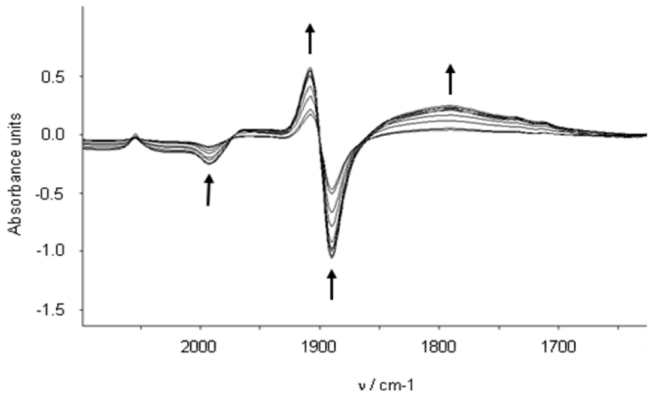

Figure 11. Difference spectra obtained in the IR region upon reduction of $[\mathbf{3a}]^{2+}$ to $[\mathbf{3a}]^{+}$ in an OTTLE cell (CH_2Cl_2, 0.2 M Bu_4NPF_6).

upon the second reduction. No concomitant emergence of weaker acetylide vibration stretches around 2040 cm^{-1} are observed as was the case with the bimetallic analogues.

NIR absorptions are often characteristic of mixed-valence compounds and can provide a powerful probe of interaction.[3] In the case of the first reduced species $[\mathbf{3a}]^{+}$, parameters extraction from the NIR absorption is difficult owing to solvent overtone. To a first approximation this band is assumed to be Gaussian, and the maximum could be located at 3800 cm^{-1}. As (i) EPR spectroscopy shows that $[\mathbf{3a}]^{+}$ is consistent with ligand-centered paramagnetic species with $S = 1/2$ (*vide supra*), (ii) chain reduction was established in the bimetallic analogues, and (iii) addition of one electron to the bis-allenylidene complex $[(Ph_2C{=}C{=}C{=})_2Ru(dppe)_2]^{2+}$ has been demonstrated to occur on both chains,[21] the present first reduction could be consistent with a class II complex involving electron delocalization over the two chains through the central ruthenium, as depicted in Scheme 2. Indeed, energy, intensity, and form are consistent with an IVCT, and Hush theory[43] reveals that the calculation $\Delta\nu_{1/2} = (2310\ \nu)^{1/2}$ cm^{-1} yields $\Delta\nu_{1/2} = 2962$ cm^{-1}. Within experimental error, this value is close to the experimental value of ca. 3070 cm^{-1} (table 4). Solvent effect was investigated with $[\mathbf{3a}]^{+}$ in acetonitrile only because of the low solubility of the compounds (Supporting Information). Spectrum analysis reveals that the band is shifted (by ~500 cm^{-1} toward higher energy) when the polarity of the medium increases, as expected for an IVCT process obeying the Hush model. However, it is worth noting that in association with the energy shift there is also an increase of the bandwidth. Furthermore, in the case of $[\mathbf{3b}]^{+}$ in CH_2Cl_2, the band shape is broader and not Gaussian (see Table 4 and Supporting Information). Thus, these observations support the idea that the band is composed of several underlying electronic excitations for both compounds. This is as well supported by DFT calculations (*vide supra*) that show that different rotamers can coexist, each of them having different absorption spectra and spin repartitions. On the one hand, partial localization could be calculated upon rotation of the two chain plans along the $C_1{-}Ru^a{-}C_1'$ axis (*vide supra*), up to 20% of extra localization on one of the two chains. Considering that all conformations could not be investigated, the presence of "class II" rotamers, assuming each chain as a redox center, is then consistent with these calculations and in line with the slight shift of the cumulenic vibration stretch to a value similar to that of bimetallic analogues upon IR monitoring. On the other hand, when full "class III" delocalization over the two halves is allowed, a fact computed for a lot of configurations, this leads to a situation comparable to that of the reduced bis-allenylidene and to the observation of a vibration stretch around 1800 cm^{-1}.[44] In addition, the presence of different rotamers implicating the C4(′)−C5(′) bonds (*vide supra*) leads to more complicated situations and spectral overlaps, explaining the unusually large bandwidth of this vibration stretch. Consequently, after the first reduction, we probably experimentally observe the superposition of several entities in solution in which the extent of electron delocalization on the carbon-rich conjugated pathway is driven by the rotations within and between the chains. Thus, the relation between the two representations of $[\mathbf{3a},\mathbf{b}]^{+}$ depicted in Scheme 2 can be viewed as mesomerism or equilibrium depending on the conformation. The extent of delocalization on one chain arbitrarily chosen as complete in this scheme would also be conformation-dependent. Importantly, given the occurrence of overlapping spectra and the unknown effective charge transferred, the apparent Hush parameters are not accurate.

Upon the second reduction, further vanishing of the visible, NIR, and IR bands are consistent with the reduction of the whole π system (Scheme 2) by comparison with reduced bimetallic analogue.[9c] Furthermore, EPR spectroscopy as well as DFT calculations suggest (i) that the two extra electrons are added on the two conjugated carbon chains, (ii) that each chain mainly bears one delocalized electron, and (iii) that the ground state is a singlet spin state with those two electrons antiferromagnetically coupled with a coupling constant on the order of kT. Thus, this coupling implies two electrons, each of them delocalized over several carbon atoms, involving the all conjugated path of the molecule in a spin polarized scheme.

Electrochemical oxidations were also performed on $[\mathbf{3a},\mathbf{b}]^{2+}$. One-electron oxidation also gives rise to a broad absorption band in the NIR region of the spectrum around 1400 nm for $[\mathbf{3a}]^{3+}$ centered at 7257 cm^{-1} (ε = 3850 $mol^{-1}\cdot L\cdot cm^{-1}$), a region in which no absorption is observed for $[\mathbf{3a}]^{2+}$ (Figure 10, Table 4). Surprisingly, the broad visible absorption is barely affected, a phenomenon already observed for related polynuclear ruthenium complexes[12g] (Table 4, Supporting Information). This confirms the multiple character of this band with a minor contribution of the transitions involving the HOMO (*vide supra*). Upon the second oxidation to $[\mathbf{3a}]^{4+}$, this absorption band decreases significantly and becomes broader. A shift of the NIR absorption band toward lower energies (λ_{max} = 5787 cm^{-1}) with increased intensity (ε = 5860 $mol^{-1}\cdot L\cdot cm^{-1}$) is also observed.[45] Upon IR monitoring of both oxidations, the vanishing of the chain contributions (ν =1880 and 1990 cm^{-1}) was gradually observed (see Supporting Information). However, the intensities of new vibrational stretches of the bridges are apparently too low to be observed, a fact already reported for other similar oxidized complexes.[7f,9c,46a,b] Solvent effect investigations for $[\mathbf{3a}]^{3/4+}$ reveal, in contrast to the reduction events, a very weak shift of the NIR bands from λ_{max} = 1378 nm (7257 cm^{-1}) to 1352 nm (7400 cm^{-1}) for $[\mathbf{3a}]^{3+}$ and from λ_{max} = 1728 nm (5787 cm^{-1}) to 1712 nm (5840 cm^{-1}) for $[\mathbf{3a}]^{4+}$ (Supporting

(43) Hush, N. S. *Prog. Inorg. Chem.* **1967**, *8*, 391–444.

(44) The reduced allenylidene $[(Ph_2C{=}C{=}C{=})_2Ru(dppe)_2]^{+\bullet}$ shows a full delocalization of the single electron over the two chains and displays a characteristic vibration stretch at 1750 cm^{-1}.

(45) Further oxidation to $[\mathbf{3a}]^{5+}$ leads to decomposition (irreversible process).

(46) (a) Winter, R. F.; Hornung, F. M. *Organometallics* **1999**, *18*, 4005–4026. (b) Winter, R. F.; Klinkhammer, K. W.; Zalis, S. *Organometallics* **2001**, *20*, 1317–1333.

Scheme 2. Proposed Lewis Formula for the First (top) and Second (bottom) Reduced Species of [**3a**,**b**]$^{2+}$

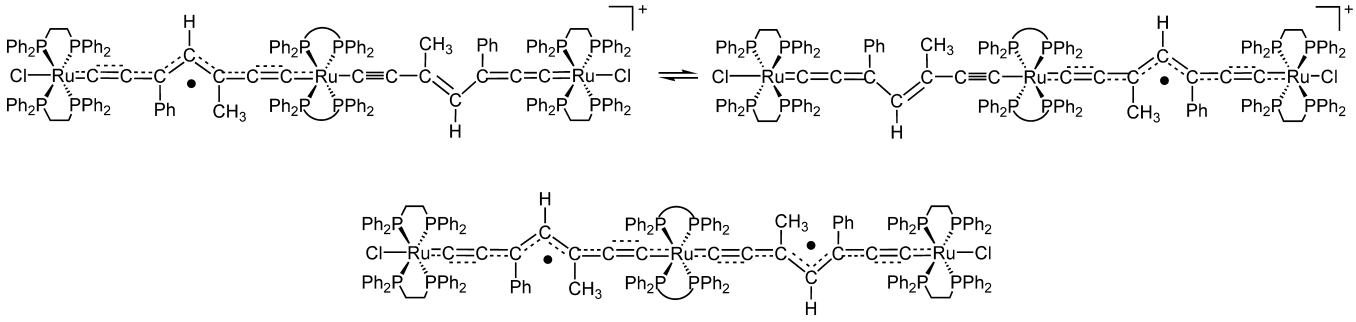

Information), indicating that the electronic coupling between the redox-active centers cannot be regarded as weak (class II).

The presence of several NIR bands in the spectra of MV complexes bearing more than two metal centers is common. Considerable complexity may be expected in the theoretical analysis of NIR transitions in trinuclear complexes due to the presence of multiple electronically coupled redox centers and to the possible presence of singlet/triplet "exciton" in addition to spin orbit coupling.[11,12c] In those MV species, deconvolutions of NIR bands usually lead to sub-bands assigned to adjacent and remote IVCT between the metal groups depending on the position of the oxidized center in the assembly.[11,15−18] With the present compounds this treatment is tempting as deconvolutions lead to two bands for [**3a**,**b**]$^{3+}$ and three bands for [**3a**,**b**]$^{4+}$ (see Supporting Information). However, their behavior strongly contrasts with that usually observed for trimetallic complexes with the fact that [**3a**]$^{4+}$ presents NIR absorptions at lower energy in comparison with those of [**3a**]$^{3+}$, which is not expected upon oxidation.[14,16] Furthermore, the involvement of both the metals and the chains makes the use of Hush theory unlikely for these absorptions that are in fact not intervalence charge transfer bands (*vide supra* and Figure S15 in Supporting Information).[3b,47] Indeed, they are due to transitions between spin orbitals, including the highest SOMOs, which are heavily carbon rich ligand centered in a complicated orbital frontiers manifold (high density of states with close nodal properties, see Figure 2). Additionally, concerning the first oxidation, EPR study also points out the fact that this process is far to be fully metal centered and involves mainly the organic ligand(s). This fact is also supported by theoretical calculations which suggest implication of the two carbon-rich chains and of the three metal atoms, and thus of the all conjugated path in the delocalization of the single electron in [**3a**,**b**]$^{3+}$ (Table 3). The data also carry out the idea that the two oxidations are not simply the successive oxidations of the two independent chains in [**3a**,**b**]$^{4+}$. In particular, the second oxidized species is EPR silent, suggesting a singlet ground state with a large S/T gap. Accordingly, DFT results indicate (i) that this state is an antiferromagnetic state, with a coupling exchange on the order of 4 kT and (ii) that this coupling occurs between two electrons, each of them being delocalized over each half, implying all the carbon atoms and metal atoms and thus the all conjugated path of the molecule.

(47) Launay, J.-P.; Coudret, C.; Hortholary, C. *J. Phys. Chem. B* **2007**, *111*, 6788–6797.

Concluding Remarks

The reported complexes [**3a**,**b**](OTf)$_2$ represent a new type of redox-active homonuclear carbon-rich molecular wires bearing more than two highly coupled metal centers of the same type. Owing to a remarkable behavior involving the three metal centers and the two non-innocent carbon-rich ligands as part of the redox system, these arrangements give rise to a fully delocalized extended structure in five oxidation states.

Specifically, these ruthenium complexes were found to be stable in two reduction and two oxidation processes that can be observed voltammetrically. The resulting states [**3a**,**b**]$^{n+}$ (n = 0−4) were characterized by UV−vis−NIR and IR spectroelectrochemical methods and EPR spectroscopy, and their geometries were modeled using DFT calculations. Reduction processes affect concomitantly both carbon chains. Upon one-electron reduction (n = 1), the single electron is delocalized over the two carbon chains through the central metal atom to an extent driven by the rotations within and between the chains. The second reduction (n = 0) implies the all conjugated path of the molecule in a spin polarized scheme: each chain conveys one electron, and the two electrons are antiferromagnetically coupled with a coupling on the order of kT. Interestingly, oxidation processes strongly involve both the metal atoms and the bridging ligands. The combined investigations reveal that the mono-oxidized systems (n = 3) presents a spin density uniformly distributed on the metal atoms and the carbon atoms of the chains, whereas when n = 4, the compounds show a strong antiferromagnetic coupling on the order of 4 kT between the two single electron localized in two distinct delocalized spin orbitals that present similar nodal properties, implying all the carbon atoms of the bridges and the metal atoms. It is worth to note that the variation of diphosphine ligands (dppe/dppm) on the central ruthenium atom does not lead to significant differences.

In this work, EPR spectroscopy turned out to be a particularly valuable tool, in agreement with DFT calculated spin densities; it revealed ligand-based spins for the reduced states and a significant participation of both the carbon-rich ligands and the metal atoms in spin delocalization upon oxidations. They illustrate the remarkable alternatives for intramolecular electron delocalization and coupling.

In common bimetallic coordination complexes, oxidation or reduction are mainly viewed as metal-centered redox processes consisting of the addition or the removal of an electron on one of the terminal metal atom to generate the mixed valence state, while the bridge serves as the conduit. For several years now, it has been well recognized that the electronic structure of the bimetallic mixed valence compounds is highly dependent on the bridging ligand nature and on the metallic building blocks.[38] In many organometallic complexes the mixing of metal and

bridging ligand orbitals was found to involve significantly this ligand in the redox events. Furthermore, different authors[48,12e,49,50] reported bimetallic complexes with unsaturated bridges that dominate the anodic redox processes. Thus, in those systems (1) the presence of the metal moieties endows the oxidized or reduced bridge with stabilities that are usually not encountered in their purely organic counterparts, and (2) the bridge is a non-innocent redox ligand that cannot be decoupled from the metal in the redox processes. For the first time, we fully demonstrate that these notions can be expanded to longer trimetallic oligomeric carbon-rich systems, and in the present examples, the metal atoms and the intervening bridging ligands provide a conduit of approximately 28 Å for electron transfer and coupling, either in an oxidation or a reduction process.[51]

Owing to the potential ability of this bimetallic system for *trans* chlorine atom substitution with another carbon-rich chain, it remains to be investigated whether even more extended and complex configurations involving non-innocent bridging ligands can be constructed.

Experimental Section

General Comments. The reactions were carried out under an inert atmosphere using the Schlenk techniques. Solvents were freshly distilled under argon using standard procedures. Electrochemical studies were carried out under argon using an Eco Chemie Autolab PGSTAT 30 potentiostat (CH_2Cl_2, 0.2 M Bu_4NPF_6); the working electrode was a Pt disk and ferrocene the internal reference. $[(dppe)_2RuCl](OTf)$,[52] $[(dppe)_2(Ru-C\equiv C-C\equiv C-SiMe_3)_2]$ (**1a**),[10e] and $[(dppm)_2(Ru-C\equiv C-C\equiv C-SiMe_3)_2]$ (**1b**)[53] were prepared as previously reported.

Spectroelectrochemistry. UV−vis−NIR spectroelectrochemistry (SEC) experiments were performed at 20 °C, under argon, with a homemade optically transparent thin-layer electrosynthetic (OTTLE) cell, path length =1 mm, using a Varian CARY 5000 spectrometer and an EG&G PAR model 362 potentiostat. A Pt mesh was used as the working electrode, a Pt wire as the counter electrode, and an Ag wire as a pseudoreference electrode. The electrodes were arranged in the cell such that the Pt mesh was in the optical path of the quartz cell. The anhydrous freeze−pump−thaw degassed sample-electrolyte solution (0.2 M *n*-Bu_4NPF_6) was cannula-transferred under argon into the cell previously thoroughly deoxygenated. Stable isosbestic points were observed during oxidation or reduction. At the end of the experiments, the original spectra were regenerated (ca. 75% optical yield for two successive one-electron processes and ca. 95% for the mono-oxidations). In every case re-reduced or re-oxidized samples displayed in the spectral region of interest no features other than those of the parent material. IR experiments were performed in similar conditions using a modified cell with KBr windows and a Bruker IFS28 spectrometer.

EPR Spectroscopy. Experiments were performed on an ESP300E (Bruker) spectrometer operating at X-band (9.3−9.8 GHz) and equipped with a rectangular TE102 resonator. Variable temperature measurements were performed with the help of an ESR900 (Oxford Instruments) continuous flow He cryostat. Because of the short lifetime of the samples and the difficulties in generating the various ionic species, it was not possible in most cases to insert a thermocouple close to the solution area. Therefore, temperature is given by the thermocouple of the temperature controller. This is expected to deviate from actual sample temperature above ca. 50 K depending on He gas flow rate. However, overall trends are not affected by such uncertainty. Electrolysis was performed within homemade two-electrode cells. Special cells were designed for potassium mirror reductions. These allowed working under secondary vacuum within a two-finger cell ending with an EPR sample tube on one side and with an UV−vis cell on the opposite side.

Computational Details. DFT calculations were performed with the Amsterdam Density Functional package (ADF 2007.01 and ADF 2009.01)[54] on slightly simplified models of $[\mathbf{3a}]^{n+}$ ($n = 0-4$), namely, $[\mathbf{3a}\text{-H}]^{n+}$, in which the phenyl groups of the phosphine ligands were replaced by hydrogen atoms (dppe → dpe, diphosphinoethane). The singlet and triplet states were considered for the neutral and tetracationic systems. In order to estimate the magnetic coupling in the latter, a broken symmetry calculation was performed leading to a mixed spin state representing the antiferromagnetic singlet state. The geometries were fully optimized without any constraint (C_1 symmetry). The Cartesian coordinates and bonding energies of each structure are given in Table S3 in Supporting Information. Because of the size of the molecules and thus of computational limits, vibrational frequencies were not calculated, but geometry optimization convergence criteria were more drastic than default ones (energy change <0.0005 hartree, atomic position displacement <0.005 Å). Electron correlation was treated within the local density approximation (LDA) in the Vosko−Wilk−Nusair parametrization.[55] The nonlocal corrections of Becke and Perdew were added to the exchange and correlation energies, respectively (BP86).[56] The analytical gradient method implemented by Verluis and Ziegler was used.[57] The standard ADF TZP basis set was used, i.e., triple-ξ STO basis set for the valence core augmented with a 3d polarization function for C, P. Orbitals up to 1s, 2p, and 4p were kept frozen for C, P, and Ru, respectively. The magnetic coupling constants of $[\mathbf{3a}\text{-H}]^{0/4+}$ were calculated following the procedure of Ruiz and co-workers.[34] They have shown that the B3LYP functional[58] is one of the best suited functional to estimate J values when spin projection cannot be handled. The resulting formula to calculate the magnetic coupling is $J_{ab} = E^{BS} - {}^3E^{HS}$ ($\hat{H}_{spin} = -J_{ab}\hat{S}_a\hat{S}_b$).[59] The excitation energies and associated oscillator strengths were calculated following the TD-DFT procedure described by van Gisbergen and co-wokers on the BP86 optimized structures.[60] In that case, the functional used was revPBE.[61] Representations of the molecular structures, orbitals, and

(48) (a) Maurer, J.; Winter, R. F.; Sarkar, B.; Fiedler, J.; Zalis, S. *Chem. Commun.* **2004**, 1900–1901. (b) Maurer, J.; Sarkar, B.; Schwederski, B.; Kaim, W.; Winter, R. F.; Zalis, S. *Organometallics* **2006**, *25*, 3701–3712.

(49) (a) Fabre, M.; Jaud, J.; Hliwa, M.; Launay, J.-P.; Bonvoisin, J. *Inorg. Chem.* **2006**, *45*, 9332–9345. (b) Chisholm, M. H.; D'Acchioli, J. S.; Hadad, C. M.; Patmore, N. J. *Inorg. Chem.* **2006**, *45*, 11035–11042. (c) Ward, M. D.; McCleverty, J. A. *J. Chem. Soc., Dalton Trans.* **2002**, *3*, 275–288.

(50) (a) Maity, N. A.; Sarkar, B.; Niemeyer, M.; Sieger, M.; Duboc, C.; Zalis, S.; Kaim, W. *Dalton Trans.* **2008**, 5749–5753. (b) Kumbhakar, D.; Sarkar, B.; Maji, S.; Mobin, S. M.; Fiedler, J.; Urbanos, F. A.; Jimnez-Apancio, R.; Kaim, W.; Lahiri, G. K. *J. Am. Chem. Soc.* **2008**, *130*, 17575–17583. (c) Ghumaan, S.; Sarkar, B.; Maji, S.; Puranik, V. G.; S. M.; Fiedler, J.; Urbanos, F. A.; Jimnez-Apancio, R.; Kaim, W.; Lahiri, G. K. *Chem.−Eur. J.* **2008**, *14*, 10816–10828. (d) Kar, S.; Sarkar, B.; Ghumaan, S.; Janardanan, D.; van Slageren, J.; Fiedler, J.; Puranik, V. G.; Sunoj, R. B.; Kaim, W.; Lahiri, G. K. *Chem.−Eur. J.* **2005**, *11*, 4901–4911.

(51) It is worth noting that investigation of long-distance intervalence electron transfer has been shown to reach a detection limit at a metal-to-metal distance of approximately 25 Å in bimetallic complexes; see ref 3e.

(52) Higgins, S. J.; La Pensée, A.; Stuart, C. A.; Charnock, J. M. *Dalton Trans.* **2001**, 902–910.

(53) Dahlenburg, L. *J. Organomet. Chem.* **1997**, *541*, 465–471.

(54) (a) te Velde, G.; Bickelhaupt, F. M.; Fonseca Guerra, C.; van Gisbergen, S. J. A.; Baerends, E. J.; Snijders, J. G.; Ziegler, T. *J. Comput. Chem.* **2001**, *22*, 931–967. (b) Fonseca Guerra, C.; Snijders, J. G.; te Velde, G.; Baerends, E. J. *Theo. Chem. Acc.* **1998**, *99*, 391–403. (c) *ADF 2007.01*; Theoretical Chemistry, Vrije Universiteit: Amsterdam, The Netherlands; SCM, www.scm.com.

(55) Vosko, S. D.; Wilk, L.; Nusair, M. *Can. J. Chem.* **1990**, *58*, 1200–1211.

(56) (a) Becke, A. D. *Phys. Rev. A* **1988**, *38*, 3098–3100. (b) Perdew, J. P. *Phys. Rev. B* **1986**, *33*, 8822–8824.

(57) Versluis, L.; Ziegler, T. *J. Chem. Phys.* **1988**, *88*, 322–328.

(58) (a) Miehlich, B.; Savin, A.; Stoll, H.; Preuss, H. *Chem. Phys. Lett.* **1989**, *157*, 200–206. (b) Lee, C.; Yang, W.; Parr, R. G. *Phys. Rev. B.* **1988**, *37*, 785–789. (c) Becke, A. D. *J. Chem. Phys.* **1993**, *98*, 5648–5652.

spin densities were done using MOLEKEL4.3[62] and ADF-GUI.[63] The structure with "W"-shaped chains of [**3a**-H]$^{2+}$ was obtained by the geometry optimization of an idealized structure obtained from the coupling of two structures [**4a**-H]$^{+}$.[9c] The starting torsion angle between the two chains was of 0°. In the optimized geometry, this angle ends up being −61°. In the case of the monoreduced and mono-oxidized species [**3a**-H]$^{+/3+}$, several starting structural arrangements and guess densities were tested in order to evaluate the capacity of localization of the unpaired electron. In each system considered, an asymmetrical guess density was chosen in order to allow the localization of the unpaired electron on one of the halves of the molecule. The geometrical arrangements investigated starting from the "W"-shaped chains optimized for [**3a**-H]$^{2+}$ were of three types: (1) modification of the torsion angle between the two "W" chains (by steps of 30°), (2) rotations of the Ru(dpe)$_2$ units, and (3) rotations along the $C_5'-C_4'$ and $C_4'-C_3'$ bonds of one of the chains (by steps of 30°). In many cases, the geometry optimization procedures lead to equivalent structures, thus only a few distinct geometries were found and reported herein. These distinct geometries obtained for [**3a**-H]$^{+/3+}$ were used as starting geometries for [**3a**-H]$^{2+}$, but only two were found different than the structure with "W"-shaped chains originally obtained.

***trans*-[Cl(dppe)$_2$Ru=C=C=C(CH$_3$)Ph](OTf) ([2a](OTf)).** In a Schlenk tube containing [(dppe)$_2$RuCl](OTf) (400 mg, 0.37 mmol) and Ph(CH$_3$)C(OH)−C≡CH (118 mg, 0.80 mmol) was added CH_2Cl_2 (40 mL). The solution was stirred for 18 h at room temperature. After filtration, the solution was evaporated, and the residue was washed with diethyl ether (3 × 25 mL). Further crystallization in a dichloromethane/pentane mixture led to dark crystals (417 mg, 86%). $^{31}P\{^1H\}$ NMR (121 MHz, $CDCl_3$, TMS): δ 41.04 (s, PPh_2). ^1H NMR (300 MHz, $CDCl_3$, TMS): δ 7.80−6.90 (m, 45H, Ph), 2.80−3.3 (m, 8 H, CH_2), 1.63 (s, 3H, CH_3). $^{13}C\{^1H\}$ NMR (75 MHz, CD_2Cl_2, TMS): δ 310.10 (quint., C_α, ^2J(P,C) = 14 Hz), 209.62 (s, C_β), 162.90 (s, C_γ), 142.48−127.83 (Ph), 125.36 (quad., CF_3, ^1J(F,C) = 321 Hz), 31.54 (CH_3), 28.67 (CH_2, $|^1J_{(P,C)} + {}^3J_{(P,C)}|$ = 23 Hz). IR (KBr): ν_{max}/cm^{-1} 1933 (=C=C=C). HR-MS FAB$^+$ (*m*/*z*): 1061.2065 ([M]$^+$, calcd 1061.2079). Analysis for $C_{63}H_{56}F_3ClO_3P_4SRu$: C 62.13, H 4.70, S 2.46 (Calcd: C 62.50, H 4.66, S 2.65).

***trans*-[Cl(dppe$_2$)Ru=C=C=C(Ph)−CH=C(CH$_3$)−C≡C−Ru(dppe$_2$)−C≡C−C(CH$_3$)=CH−C(Ph)=C=C=Ru(dppe$_2$)Cl][2TfO]$_2$ ([3a](OTf)$_2$).** In a Schlenk tube, a solution of [**2a**](OTf) (242 mg, 0.2 mmol) in CH_2Cl_2 (30 mL) was added to a solution of **1a** (114 mg, 0.1 mmol) in CH_2Cl_2 (30 mL). The addition was carried out slowly (51 h) using a dropping funnel. The mixture was further stirred for 4 days at room temperature. After filtration, the solution was evaporated, and the residue was washed with diethylether (2 × 20 mL) and then dried under vacuum. Further crystallizations in a methylene chloride/pentane mixture led to blue crystals (177 mg, 52%). The following labeling is used for NMR peak attributions: [Ru^a]=C$_1$=C$_2$=C$_3$(Ph)−C$_4$H=C$_5$(CH$_3$)−C$_6$≡C$_7$−[Ru^b]−C≡C−C(CH$_3$)=CH−C(Ph)=C=C=[Ru^a]. $^{31}P\{^1H\}$ NMR (121 MHz, CD_2Cl_2): δ 51.63 (s, PPh_2 dppe), 44.90 (s, PPh_2 dppe). ^1H NMR (300 MHz, CD_2Cl_2): δ 7.64−6.99 (m, 126H, Ph), 6.82 (d, 4H, $^3J_{(H,H)}$ = 7.4 Hz, CH phenyl chain), 5.76 (s, 2H, C=CH−C), 2.90 (m, 8 H, CH_2), 2.67 (m, 16 H, CH_2), 0.89 (s, 6H, CH_3). $^{13}C\{^1H\}$ NMR (75 MHz, CD_2Cl_2): δ 260.60 (quint., Ru^a=C_1, $^2J_{(P,C)}$ = 14 Hz), 193.02 (quint., Ru^b−C_7, $^2J_{(P,C)}$ = 14 Hz), 182.80 (s, Ru^a=C=C_2), 156.36 (s, Ru^b−C≡C_6), 149.01 (s, Ru^b−C≡C−C_5), 146.63 (s, Ru^a=C=C=C_3), 136.97 (s, Ru^a =C=C=C−C_4H), 145.58−127.77 (Ph), 31.31 (quint., CH_2 dppe Ru^b, $|^1J_{(P,C)} + {}^3J_{(P,C)}|$ = 23 Hz), 28.82 (quint., CH_2 dppe Ru^a, $|{}^1J_{(P,C)} + {}^3J_{(P,C)}|$ = 23 Hz), 24.07 (s, CH_3). IR (KBr): ν_{max}/cm^{-1} 1987 (C≡C, weak), 1884 (=C=C=C, strong). HR-MS FAB$^+$ (*m*/*z*): 1559.3056 ([M]$^{+2}$, calcd 1559.3018). Analysis for $C_{186}H_{162}Cl_2P_{12}Ru_3F_6O_6S_2$: C 64.97, H 4.69 (Calcd: C 65.38, H 4.78).

***trans*-[Cl(dppe$_2$)Ru=C=C=C(Ph)−CH=C(CH$_3$)−C≡C−Ru(dppm$_2$)−C≡C−C(CH$_3$)=CH−C(Ph)=C=C=Ru(dppe$_2$)Cl][2TfO]$_2$ ([3b](OTf)$_2$).** In a Schlenk tube, a solution of [**2a**](OTf) (242 mg, 0.2 mmol) in CH_2Cl_2 (30 mL) was added to a solution of **1b** (111 mg, 0.1 mmol) in CH_2Cl_2 (30 mL). The addition was carried out slowly (51 h) using a dropping funnel. The mixture was further stirred for 12 days at room temperature. After filtration, the solution was evaporated, and the residue was washed with diethylether (2 × 20 mL) and then dried under vacuum. Further crystallizations in a methylene chloride/pentane mixture led to blue crystals (193 mg, 57%). The following labeling is used for NMR peak attributions: [Ru^a]=C$_1$=C$_2$=C$_3$(Ph)−C$_4$H=C$_5$(CH$_3$)−C$_6$≡C$_7$−[Ru^c]−C≡C−C(CH$_3$)=CH−C(Ph)=C=C=[Ru^a]. $^{31}P\{^1H\}$ NMR (121 MHz, CD_2Cl_2): δ −6.27 (s, PPh_2 dppm), 43.30 (s, PPh_2 dppe). ^1H NMR (300 MHz, CD_2Cl_2): δ 7.60−6.77 (m, 126H, Ph), 6.52 (d, 4H, $^3J_{(H,H)}$ = 7.2 Hz, CH phenyl chain), 5.51 (s, 2H, C=CH−C), 5.04 (m, 4 H, CH_2 dppm), 2.92 (m, 8 H, CH_2 dppe), 2.64 (m, 8 H, CH_2 dppe), 0.52 (s, 6H, CH_3). $^{13}C\{^1H\}$ NMR (75 MHz, CD_2Cl_2): δ 255.09 (quint., Ru^a=C_1, $^2J_{(P,C)}$ = 13 Hz), 195.26 (quint., Ru^c−C_7, $^2J_{(P,C)}$ = 14 Hz), 176.47 (s, Ru^a=C=C_2), 155.18 (s, Ru^c−C≡C_6), 151.57 (s, Ru^c−C≡C−C_5), 147.27 (s, Ru^a=C=C=C_3), 136.37 (s, Ru^a =C=C=C−C_4H), 146.07−127.44 (Ph), 50.51 (quint., CH_2 dppm, $|^1J_{(P,C)} + {}^3J_{(P,C)}|$ = 25 Hz), 28.11 (quint., CH_2 dppe, $|^1J_{(P,C)} + {}^3J_{(P,C)}|$ = 22 Hz), 23.07 (s, CH_3). IR (KBr): ν_{max}/cm^{-1} 1994 (C≡C, weak), 1890 (=C=C=C, strong). HR-MS FAB$^+$ (*m*/*z*): 1545.7922 ([M]$^{+2}$, calcd 1545.7898). Analysis for $C_{184}H_{158}Cl_2P_{12}Ru_3F_6O_6S_2$: C 64.99, H 4.81, S 1.93 (Calcd: C 65.21, H 4.70, S 1.89).

Acknowledgment. We thank the CNRS and the Université de Rennes 1 for support and the Ministère de la Recherche for a Ph.D. grant to C.O.; J.-Y.S. and K.C. thank the French computing centers IDRIS-CNRS and CINES for computational facilities; J.-Y.S. thanks the IUF for financial support.

Supporting Information Available: Mesomeric schemes, additional EPR spectroscopy, spectroelectrochemical data for [**3a,b**]$^{n+}$, and theoretical results. This material is available free of charge via the Internet at http://pubs.acs.org.

JA908948G

(59) (a) Nishino, M.; Yamanaka, S.; Yoshioka, Y.; Yamaguchi, K. *J. Phys. Chem. A* **1997**, *101*, 705–712. (b) Yamaguchi, K.; Fukui, H.; Fueno, T. *Chem. Lett.* **1986**, *15*, 625–628. (c) Ruiz, E.; Alvarez, S.; Cano, J.; Polo, V. *J. Chem. Phys.* **2006**, *124*, 107102.

(60) van Gisbergen, S. J. A.; Snijders, J. G.; Baerends, E. J. *Comput. Phys. Commun.* **1999**, *118*, 119–138.

(61) (a) Perdew, J. P.; Burke, K.; Ernzerhof, M. *Phys. Rev. Lett.* **1996**, *77*, 3865–3868. (b) Hammer, B.; Hansen, L. B.; Norskov, J. K. *Phys. Rev. B* **1999**, *59*, 7413–7421.

(62) Flükiger, P.; Lüthi, H. P.; Portmann, S.; Weber, J. *Molekel 4.3*; Swiss Center for Scientific Computing: Manno, 2002.

(63) *ADF-GUI 2008.01 and 2009.01*; SCM: Amsterdam, The Netherlands; www.scm.com.